Dynamics in the H_2^+ molecule, using a one dimensional model

Sigurd Askeland

Thesis for the degree of Master of Science

University of Bergen, Norway
Department of Physics and Technology
2009

Forord

Eg sender ei stor takk til Morten Førre, som rettleia meg gjennom masterarbeidet på ypperleg vis. Han har (minst) tre eigenskapar ein drøymer om i ein rettleiar: tolmod, godt humør og alltid nokre minuttar til å forklara noko. PhD-studentane nede i gangen, Lene Sælen, Tore Birkeland og Raymond Nepstad, har alltid tatt seg tid til å hjelpa ein masterstudent som møter veggen. Tusen takk for det. Ein må for all del ikkje gløyma Sigrid Ina Simonsen, Arne Skodvin Kristoffersen og Stian Astad Sørngård, som skaper den flotte stemninga på kontoret. Heilt på tampen går ei takk til min venn og matematikar Sveinung Cornelius Fjær for djupe samtalar i badstova.

Bergen, juni 2009

Sigurd Askeland

Contents

Chapter 1

Introduction

Quantum mechanics was born when Max Planck found the quantisation of light, at the dawning of the last century [1]. The birth was not planned for, but nurturing parents such as Einstein, de Broglie and Bohr took excellent care of the baby, and it thrived and put on weight. Perhaps Heißenberg introducing matrix mechanics can be described as the toddeler's first steps, but it spoke its first words (probably in German) when the Schrödinger equation was put forth by Erwin Schrödinger in 1926. Quantum mechanics has since then matured into an important tool used in many branches of both physics and chemistry. It is at the root of atomic, molecular, nuclear and particle physics. For any deeper understanding of chemistry you will need it. It plays a vital role in astrophysics, nor can it be ignored as microelectronics strive to become nanoelectronics. Quantum mechanics has withstood rigorous testing, and is at present without doubt the best theory to describe the submicroscopic world.

Though most of the fundamental principles of quantum mechanics seems to be nailed down, its full potential cannot easily be tapped. Even what we would call simple problems such as a hydrogen molecule, H_2, is so complex when described with quantum mechanics, that they cannot be solved analytically. Atomic and molecular physics began to make strides ahead with the appearance of the first computers in the 1940s. Most often quantum mechanical problems have to be solved numerically, by approximative methods. As the computers became stronger and faster, and the algorithms more efficient, the physicisists and chemists could model larger systems, with less approximations. In 1956, scientists at MIT did the first ab initio Hartree-Fock calculations on diatomic molecules [2]. Today chemists can describe systems with dozens of electrons with some accuracy using density functional theory [3]. In parallel, the experimental technology saw a similar development.

With laser pulses of high intensity and short durations, it has now become possible to see chemical reactions in progress at a molecular level, (A. H. Zewail was awarded the Nobel prize in 1999 for his work in this area [4]), as well as controlling the state of quantum mechanical systems [5]. With high accuracy theoretical calculations of atomic and molecular systems, one is building up a better understanding of atomic/molecular processes, and how to control these [6]. This is of fundamental importance for atomic physics, quantum chemistry and for all related technology.

Molecules contain more than one nucleus, and are held together by one or more electrons. The additional freedoms of nuclear movement make molecular problems more complex than atomic systems. Dissosiation and ionisation of molecules by lasers have been studied in experiments, and recently the hydrogen molecule, H_2, have been succesfully modelled in 3D with high accuracy [7], albeit using the Born-Oppenheimer approximation, and only for weak fields. This is a huge problem, and consequently a common approach to this sort of scenarios is to reduce the dimensionality of the problem. The Born-Oppenheimer (BO) approximation is another widely used simplification, that separates the nuclear and electronic parts of the Schrödinger equation. This makes molecular problems more manageable. The approximation is based on the fact that nuclei are heavy and slow compared to the electrons. This may not always be the case for molecules in a laser field [8]. In this thesis we have studied the hydrogen molecular ion, H_2^+, by solving the Schrödinger equation. It is the simplest molecule there is, and it is therefore an ideal system to study in detail. The goal of the thesis was to design and implement a model of H_2^+. The model developed in this thesis does not describe the molecule in three dimensions, as that would be an enormous job. Instead we developed a one dimensional approximation of the molecule. It is often useful to look at a problem using a flexible, fast and cheap model, before (or in stead of) going to the trouble of modelling it in 3D. For that reason 1D models are very common [9, 10, 11, 12, 13, 14]. The success of the one dimensional model will of course depend on how well the results agree with experiments. As the model was being developed, a new approach was implemented to make the model better. Our model is based on the Born-Oppenheimer approximation, but in addition, it can include the non-Born-Oppenheimer effects. After completing the model, it was tested. Two articles, [15, 16], which report interesting results on H_2^+ calculated in 3D in the Born-Oppenheimer regime, were chosen. We attemted to reproduce some of the results from these articles with our model. Comparison then gave an idea of how well the model works. We also searched for discepancies in the results between the BO and the non-BO simulations.

The thesis will describe the development of our H_2^+ model, and the result of its testing. Preliminarily, a brief introduction is given to quantum mechanics, lasers and the hydrogen molecular ion. The Born-Oppenheimer approximation is introduced, and used to simplify the Schrödinger equation for H_2^+. We then go on to report how we modelled H_2^+ in one dimension. A chapter is devoted to the usual consepts when going to 1D, as well as our own modifications. This is followed by a few chapters that recount the actual numerics and programming solutions used when implementing the model. Ultimately we present the simulations that were run, and how they compared to the 3D scenarios.

Chapter 2

The Schrödinger equation

The time dependent Schrödinger equation (TDSE) plays much the same role in quantum mechanics as Newton's 2nd law does in regular mechanics. By solving the equation, one obtains the wavefunction, from which all attainable information about the quantum system can be extracted. The TDSE

$$i\hbar\frac{\partial\Psi}{\partial t} = \widehat{H}\Psi \tag{2.1}$$

is a partial differential equation. The Hamiltonian, $\widehat{H}$, is the energy operator, and will be different from problem to problem. i is the imaginary unit, $\hbar$ is the reduced Planck's constant and Ψ is the wavefunction. The standard interpretation of the wavefunction is as a probability distribution. If the Schrödinger equation were to be solved for an electron, for example, then $|\Psi(\vec{r},t)|^2$ is its probability density, i.e.

$$|\Psi(\vec{r},t)|^2\, d^3r$$

is the probability of measuring the electron in the voulume d^3r around the position $\vec{r}$ at the time t.

2.1 Separating out time

When the Hamiltonian of a problem is time independent, the wavefunction can be separated into a function depending only on t, and a function that is independent of t [1].

Assume $\Psi(\vec{r},t)$ can be written on the form $\Psi(\vec{r},t) = \psi(\vec{r})T(t)$. The Schrödinger equation will now take the form

$$i\hbar\psi(\vec{r})\frac{\partial T(t)}{\partial t} = T(t)\widehat{H}(\vec{r})\psi(\vec{r}) \tag{2.2}$$

Dividing on both sides by $\psi(\vec{r})T(t)$, and one is left with no time dependence on the right, and no position dependence on the left,

$$\frac{i\hbar\frac{\partial T(t)}{\partial t}}{T(t)} = \frac{\widehat{H}(\vec{r})\psi(\vec{r})}{\psi(\vec{r})} \tag{2.3}$$

For the left side to be equal to the right for all $\vec{r}$ and t, both sides have to be equal to a constant. This constant is called E, as it happens to be the energy of the system. The Schrödinger equation can now be separated into two equations,

$$i\hbar\frac{\partial T(t)}{\partial t} = ET(t) \tag{2.4}$$

and

$$\widehat{H}(\vec{r})\psi(\vec{r}) = E\psi(\vec{r}) \tag{2.5}$$

The solution to Eq. (2.4) is

$$T(t) = Ce^{\frac{-iEt}{\hbar}} \tag{2.6}$$

It is not that straight forward to find $\psi(\vec{r})$. Equation (2.5) is called the time independent Schrödinger equation, (TISE). Depending on the Hamiltonian, this equation can be anything but trivial to solve.

2.2 The hydrogen molecular ion (H_2^+)

Each particle that is included in the Schrödinger equation typically increases the dimensionality of the problem by three (disregarding spin). Faced with an exponential increase in computation costs with the number of particles, one can either use other approximative approaches, such as Hartree-Fock and Density Functional Theory[1], or one can choose problems with few particles. Having chosen the latter, a theoretical physicist is not left with many molecules. The simplest molecule that is abundant in nature, is hydrogen gas, H_2. With only two protons and two electrons, it contains the bare minimum for a neutral

[1] For more on the Hartree-Fock method and DFT, see [3].

molecule. Unfortunately, it is still a huge problem, of 9 dimensions even in the centre of mass reference frame. By removing one electron from the equation, the problem becomes more manageable. The ionised version of the gas, H_2^+, consists of two protons held together by an electron, (see Fig. 2.1). However, the full 3D solution of H_2^+ is still a formidable task, and one is very often obliged to perform further approximations. In this thesis, the TISE was solved for a model H_2^+ molecule. The Hamiltonian operator for H_2^+ in the centre of mass frame reads

$$\widehat{H} = -\frac{\hbar^2}{2m_e}\nabla^2_{\vec{r}} - \frac{\hbar^2}{2\mu}\nabla^2_{\vec{R}} - \frac{ke^2}{\left|\vec{r}+\frac{\vec{R}}{2}\right|} - \frac{ke^2}{\left|\vec{r}-\frac{\vec{R}}{2}\right|} + \frac{ke^2}{\left|\vec{R}\right|} \tag{2.7}$$

The first term represents the kinetic energy of the electron, the second term the kinetic energy of the nuclei and the potential is given by three Coulomb terms: the Coulomb attraction between the electron and each nucleus, and the Coulomb repulsion between the nuclei.

e	Proton/electron charge
$k = \frac{1}{4\pi\epsilon_0}$	where ϵ_0 is the permittivity of vacuum
m_e	Mass of the electron
M	Mass of the nucleus
$\mu = \frac{M^2}{2M} = \frac{M}{2}$	The reduced mass of the nuclei
$\hbar = \frac{h}{2\pi}$	The Planck constant over 2π
$\vec{r}$	The electron position variable
$\vec{R}$	The distance between the nuclei

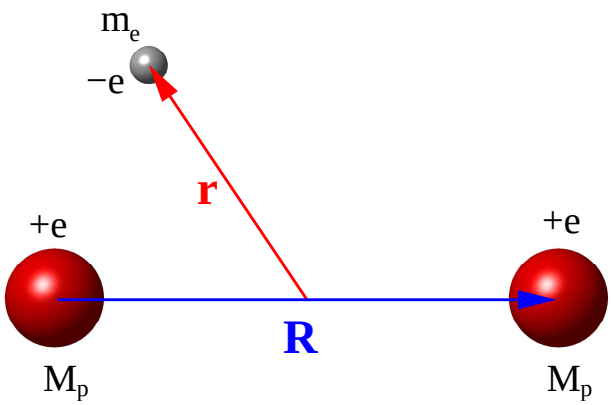

Figure 2.1: The H_2^+ molecule, consisting of two protons and an electron.

2.3 Laser

A laser emits a beam of monochromatic, coherent electromagnetic waves, i.e. the photons emitted have the same frequency and are perfectly in phase.

"Laser" is an acronym for Light Amplification by Stimulated Emission of Radiation [3]. As early as in 1916 Albert Einstein laid the theoretical foundation for lasers, with an article regarding absorption and emission of radiation [17]. It would take another 43 year until Theodore Maiman built the first working laser, in 1960 [18]. Since then lasers have been used extensively in science. Several Nobel Prizes have been awarded for work involving lasers, among them the 1997 prize, "for development of methods to cool and trap atoms with laser light" [19]. In medicine, lasers are used for surgery, while diametrically different uses are put to the technology in the military, where lasers are used for weapons targeting. The laser is put to more mundane uses as well. It enters into everyone's daily life through appliances such as the CD player, the laser printer and the bar code reader.

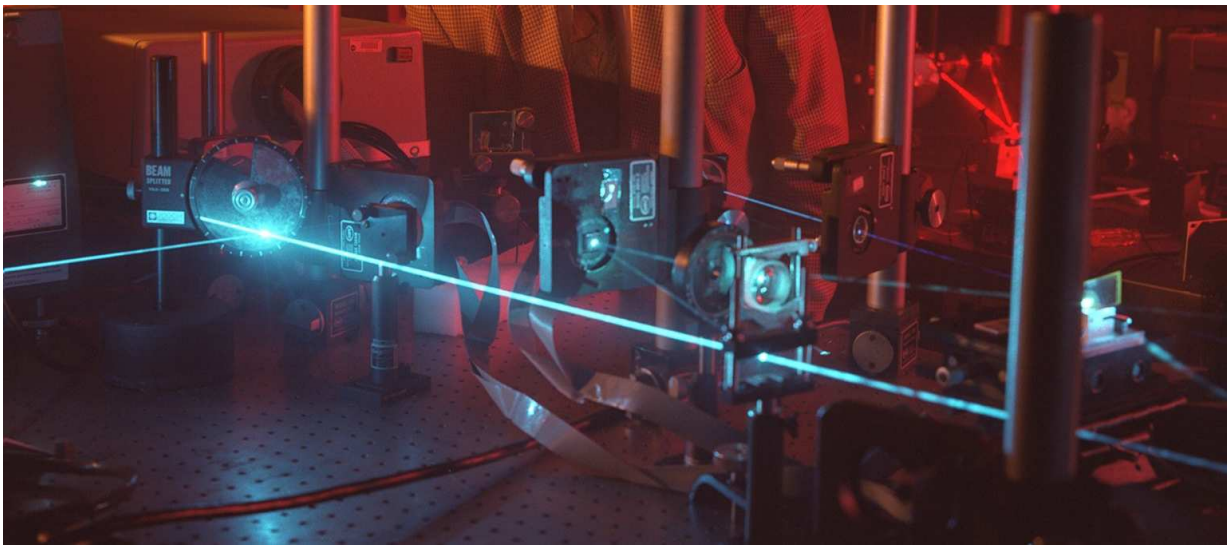

Figure 2.2: Lasers have a wide range of scientific applications. NASA/courtesy of nasaimages.org.

Lasers are of great importance in atomic and molecular physics. Short, high intensity laser pulses provide finely controlled external stimuli to atoms/molecules, thus allowing imaging of atomic systems. It even allows for controlling the state of the system [6]. This can for example be used for controlling chemical reactions [4].

In this thesis, we will model an H_2^+ molecule in a short, high intensity laser pulse, and calculate the ionisation and dissosiation spectra. That means adding an extra term to the Hamiltonian from the previous section. So far the problem has been time independent. That will not be the case when a laser field is turned on. The laser will be modelled as an electric field that changes with time, but not with position, i.e. the so called dipole approximation[2] is applied. At any time, the potential energy of a particle with charge q in a homogenous electric field will be given as

$$U = -q\vec{E}(t) \cdot \vec{r}$$

relative to origin [20]. The Hamiltonian for H_2^+ will get three more terms when the field is turned on, one for each charge. However, in the centre of mass reference frame, the two nuclear terms differ only in sign, and cancel each other out, leaving only one extra term. This means that only the electron is affected by the field, and the Hamiltonian, Eq. (2.7),

[2]The dipole approximation [3] stems from the fact that the wavelength of the laser light is much longer than the spatial extension of the molecular/atomic system, and the laser field can therefore be considered to be homogenous.

becomes

$$\widehat{H} = -\frac{\hbar^2}{2m_e}\nabla^2_{\vec{r}} - \frac{\hbar^2}{2\mu}\nabla^2_{\vec{R}} - \frac{ke^2}{\left|\vec{r}+\frac{\vec{R}}{2}\right|} - \frac{ke^2}{\left|\vec{r}-\frac{\vec{R}}{2}\right|} + \frac{ke^2}{\left|\vec{R}\right|} + e\vec{E}(t)\cdot\vec{r} \tag{2.8}$$

$E(t)$ will typically oscillate rapidly, the amplitude modulated by a carrier envelope, to model a laser pulse, (see Fig. 2.3). By controlling the laser frequencies and the intensity profile, it is to some extent possible to control the quantum system to which the pulse is applied.

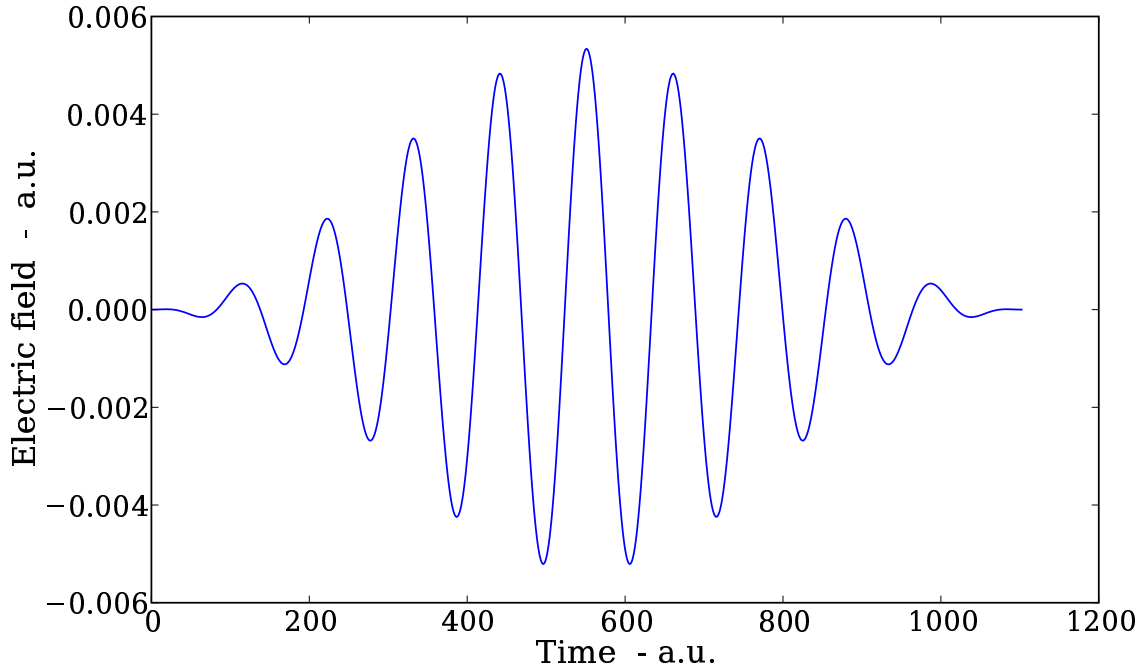

Figure 2.3: Theoretically, laser pulses are often defined by $E(t) = E_0 \sin^2(\frac{\pi t}{T})\cos(\omega t)$, where T is the pulse length, and ω is the angular frequency [16][21][22].
This example pulse contains 10 cycles of an infrared laser (800 nm), with intensity $I = 10^{12}$ Wcm^{-2}.

Chapter 3

The Born-Oppenheimer approximation

Since its conception in the late 1920s [23], the Born-Oppenheimer (BO) approximation, as it came to be called, have been extensively used in molecular physics and quantum chemistry. The BO approximation [1] allows one to seperately calculate the wavefunctions of electrons and nuclei, when solving the Schrödinger equation for molecules. Due to the large difference in mass between the electron and the nuclei (a proton weighs roughly 1836 times as much as an electron), the electrons move on a shorter time scale than the nuclei. The crudest approximation at this point would be to assume that the nuclei were fixed in one position. This is equivalent to assuming the nuclei have infinite mass. The Fixed Nuclei Approximation, (FNA), as it is called, is of course way to rigid for most problems. A more reasonable approach is to solve the Schrödinger equation for the electrons as if the nuclei were frozen in place, but doing this for a sufficient number of nuclear arrangements, so that the electrons' impact on the nuclei can be included when solving the rest of the equation.

In order to solve the equation for the nuclei separately, the electronic wavefunction must be decoupled from the *nuclear* part of the Hamiltonian. This means that the kinetic energy terms of the nuclei, i.e. the differentiation with regard to nuclear positions, must not act on the electronic wavefunction. In other words, the partial differentiations of the electronic wavefunction in the nuclear variables must be set to zero,

$$\nabla_{\vec{R}} \psi_{electron}(\vec{r}; \vec{R}) = 0$$

where $\vec{R}$ and $\vec{r}$ are the position vectors of a nucleus and an electron, respectively. The seperation significantly simplifies the task of solving the Schrödinger equation.

3.1 H_2^+ in the BO approximation

The Hamiltonian operator for H_2^+, as given in Eq. (2.7), reads

$$\widehat{H} = -\frac{\hbar^2}{2m_e}\nabla_{\vec{r}}^2 - \frac{\hbar^2}{M}\nabla_{\vec{R}}^2 - \frac{ke^2}{\left|\vec{r}+\frac{\vec{R}}{2}\right|} - \frac{ke^2}{\left|\vec{r}-\frac{\vec{R}}{2}\right|} + \frac{ke^2}{\left|\vec{R}\right|} \tag{3.1}$$

Terms with an explicit $\vec{r}$ dependence are put into an *electronic Hamiltonian*,

$$\widehat{H}_e = -\frac{\hbar^2}{2m_e}\nabla_{\vec{r}}^2 - \frac{ke^2}{\left|\vec{r}+\frac{\vec{R}}{2}\right|} - \frac{ke^2}{\left|\vec{r}-\frac{\vec{R}}{2}\right|} \tag{3.2}$$

An attempt is made to seperate the wavefunction into a function of $\vec{r}$, describing the electronic part of the system, and a function of $\vec{R}$, describing the nuclear part. A complete separation is not possible, due to the denominators in the Coulomb attraction part of the Hamiltonian. However, if one assumes that the electronic wavefunction only depends on $\vec{R}$ as a constant parametre, the total wave function can be expressed as

$$\Psi_{tot}(\vec{r},\vec{R}) = \psi_e(\vec{r};\vec{R})\chi(\vec{R}) \tag{3.3}$$

The validity of this assumption will be discussed later.

The electronic wavefunction, $\psi_e(\vec{r};\vec{R})$, can be found from the eigenvalue problem

$$\widehat{H}_e\psi_e(\vec{r};\vec{R}) = E_e(\vec{R})\psi_e(\vec{r};\vec{R}) \tag{3.4}$$

The electronic energies, $E_e(\vec{R})$, will now be functions of the nuclear distance, $\vec{R}$.

How to solve for the vibrational wavefunction of the nuclei, $\chi(\vec{R})$, becomes apparent when looking at the TISE for H_2^+:

$$\widehat{H}\Psi_{tot} = E\Psi_{tot}$$
$$\widehat{H}\psi_e(\vec{r};\vec{R})\chi(\vec{R}) = E\psi_e(\vec{r};\vec{R})\chi(\vec{R})$$

$\chi(\vec{R})$ is independent of $\vec{r}$, and is unchanged by the $\widehat{H}_e$ operator.

$$\chi(\vec{R})\widehat{H}_e\psi_e - \frac{\hbar^2}{M}\nabla_{\vec{R}}^2\left(\psi_e(\vec{r};\vec{R})\chi(\vec{R})\right) + \frac{ke^2}{|R|}\psi_e(\vec{r};\vec{R})\chi(\vec{R}) = E\psi_e(\vec{r};\vec{R})\chi(\vec{R})$$
$$\left[-\frac{\hbar^2}{M}\nabla_{\vec{R}}^2 + E_e(\vec{R}) + \frac{ke^2}{|R|}\right]\psi_e(\vec{r};\vec{R})\chi(\vec{R}) = E\psi_e(\vec{r};\vec{R})\chi(\vec{R})$$

The Laplacian,

$$\nabla^2_{\vec{R}}(\psi\chi) = \chi\nabla^2_{\vec{R}}\psi + 2\nabla_{\vec{R}}\psi \cdot \nabla_{\vec{R}}\chi + \psi\nabla^2_{\vec{R}}\chi$$

is inserted in the full equation,

$$-\frac{\hbar^2}{M}\left(\psi_e(\vec{r};\vec{R})\nabla^2_{\vec{R}}\chi(\vec{R}) + 2\nabla_{\vec{R}}\psi_e(\vec{r};\vec{R}) \cdot \nabla_{\vec{R}}\chi(\vec{R}) + \chi(\vec{R})\nabla^2_{\vec{R}}\psi_e(\vec{r};\vec{R})\right) + \left(E_e(\vec{R}) + \frac{ke^2}{|R|}\right)\psi_e(\vec{r};\vec{R})\chi(\vec{R}) = E\psi_e(\vec{r};\vec{R})\chi(\vec{R})$$

At this point, one uses the Born-Oppenheimer approximation. Simply stated, the differensiations of $\psi_e(\vec{r};\vec{R})$ with respect to R is considered negligible, i.e.

$$\nabla^2_{\vec{R}}\psi_e(\vec{r};\vec{R}) = 0$$
$$\nabla_{\vec{R}}\psi_e(\vec{r};\vec{R}) = 0$$

The approximation relies on the fact that electrons are so much lighter than the nuclei, that they have time to adjust adiabatically to the nuclear movement. While the nuclear wavefunctions typically have a lot of oscillations, (as the electronic wavefunctions have in the x domain), the electronic wavefunctions have only a slow and smooth dependence on R. As a consequence,

$$\left|\nabla_{\vec{R}}\psi_e(\vec{r};\vec{R})\right| << \left|\nabla_{\vec{R}}\chi(\vec{R})\right|$$

When this is used, the equation is greatly simplified,

$$-\frac{\hbar^2}{M}\left(\psi_e(\vec{r};\vec{R})\nabla^2_{\vec{R}}\chi(\vec{R})\right) + \left(E_e(\vec{R}) + \frac{ke^2}{|R|}\right)\psi_e(\vec{r};\vec{R})\chi(\vec{R}) = E\psi_e(\vec{r};\vec{R})\chi(\vec{R}) \tag{3.5}$$

The electronic wavefunction, $\psi_e(\vec{r};\vec{R})$, becomes a common factor, and cancels, leaving

$$\left[-\frac{\hbar^2}{M}\nabla^2_{\vec{R}} + E_e(\vec{R}) + \frac{ke^2}{|R|}\right]\chi(\vec{R}) = E\chi(\vec{R}), \tag{3.6}$$

an $\vec{r}$ independent eigenvalue problem, that can be calculated numerically. Notice how the electronic energies calculated in Eq. (3.4), now set up an effective potential in the vibrational Hamiltonian, Eq. (3.6). The eigenvalue, E, is the total energy of the state, $\Psi_{tot}(\vec{r},\vec{R})$, i.e. the sum of the electronic energy, the vibrational energy and the rotational energy.

The electronic energy is typically much larger than the vibrational energy, which again

is two or three orders of magnitude larger than the rotational energy[1]. This leads to the differences in timescales between nuclei and electrons, which made a separation of their wavefunctions possible. There is a similar difference in the typical time periods of nuclear vibration and rotation [22],

$$t_{electron} \approx 10^{-18}s, \quad t_{vibration} \approx 10^{-15}s, \quad t_{rotation} \approx 10^{-12}s \tag{3.7}$$

meaning vibrational and rotational motion can be separated as well. In this thesis the rotation is in fact completely ignored, since the entire time propagation of the Schrödinger equation will be of the order 10 fs. That means the nuclei are set with a certain orientation, and only allowed to move along the internuclear axis. This approximation eases the work load, since the electronic wave equation, Eq. (3.4), needs only be solved for $\vec{R}$ values in one dimension.

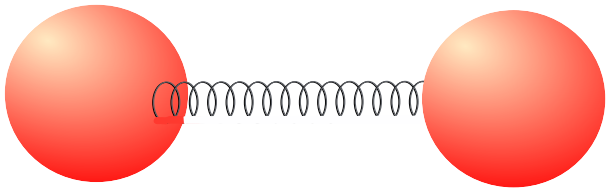

Figure 3.1: Vibration typically has a time period of the order of 10^{-15} s.

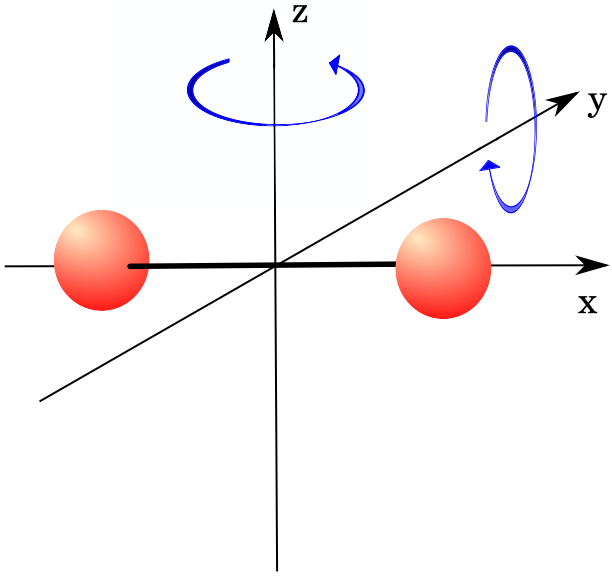

Figure 3.2: Rotation typically has a time period of the order of 10^{-12} s.

[1] These results are derived in [3] pp. 477–480.

3.2 Processes in H_2^+

In the BO approximation, the wavefunction separates into an electronic and a vibrational wavefunction. Frequently, one meets the problem visualised by a drawing of the potential in the nuclear Hamiltonian, Eq. (3.6). As one is using the reduced mass in the center of mass reference frame, the vibrational wave equation describes the nuclei as *one* particle in a potential of the form

$$V = E_e(R) + \frac{1}{R}$$

where $E_e(R)$ are the energies of the electron, calculated from Eq. (3.4). That makes it possible to have a classical intuition of how the system will behave. Figure 3.3 shows the energy curves for the 3D model.

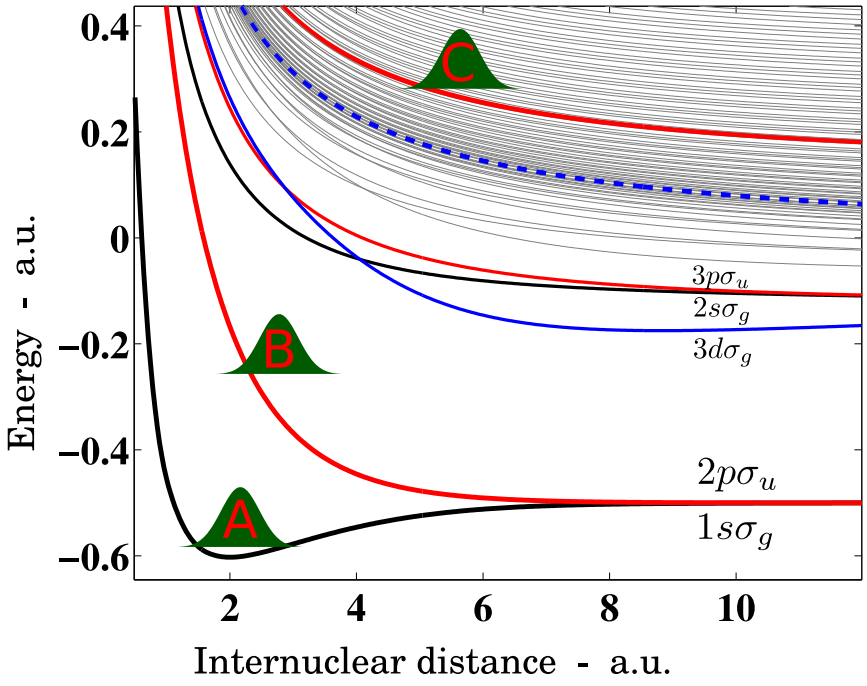

Figure 3.3: Electronic energy curves in H_2^+. The names of the lowest curves are included. Three different wavepackets are drawn schematically on the figure. Wavepacket **A** is composed mainly of bound states, and the molecule will stay together. Wavepacket **B** is made of dissosiating states, i.e. the molecule will divide into a proton and a hydrogen atom. The energy curves which wavepacket **C** belongs to is above the ionisation threshold (dashed line), i.e. the electronic energy is greater than 0. With time the molecule will split into two protons and an electron.

The names of the curves are inherited from the states of He^+, i.e. H_2^+ in the limit of $R \to 0$. $1s\sigma_g$, e.g., corresponds to the ground state in the Helium ion. The number 1 is the

principal quantum number, the s signifies the angular momentum quantum number $l = 0$, the σ indicate the l_z quantum number $m_l = 0$, and the g stands for *gerade*, meaning the electronic wavefunction is even about the origin. Similarly for $2p\sigma_u$, the state is described by $n = 2, \quad l = 1, \quad m_l = 0$ and the u stand for *ungerade*, or odd. In the figure, three wavepackets have been drawn, labelled **A**, **B** and **C**. The packets will demonstrate the three possible fates of a diatomic molecule. To a certain extent, the wavepackets on a potential curve will behave as if it were a ball on a slope. Since the nuclear state is typically just excited from the ground state, the probability density often retains the localised character of a wavepacket. It is therefore not all that inaccurate to envisage the wavepacket as a classical particle. The "particle" will slide down the inclined curve, exchanging potential energy for kinetic energy. In the case of wavepacket **A**, the packet will regain the potential energy on the opposite slope of the potential curve, and return, since the packet resides near a minimum. The system is composed of bound states. In such cases, the internuclear distance will not diverge, i.e. one has a stable molecule. For wavepacket **B**, there is no opposite slope, and the wavepacket will slide off into the unknown. This means that the nuclei are drifting apart. However, the electron will stay bound to one of the protons. This process is called dissosiation, and the result in this case is a free proton and a hydrogen atom (in the $1s$ state). Wavepacket **C** is above the ionisation threshold, (the dashed curve in Fig. 3.3), meaning the electron has a positive energy. As a consequence, not only will the nuclei drift apart, but the electron will no longer be bound, and will travel off without any of its molecular companions. This is called a Coulomb explosion (CE), or ionisation.

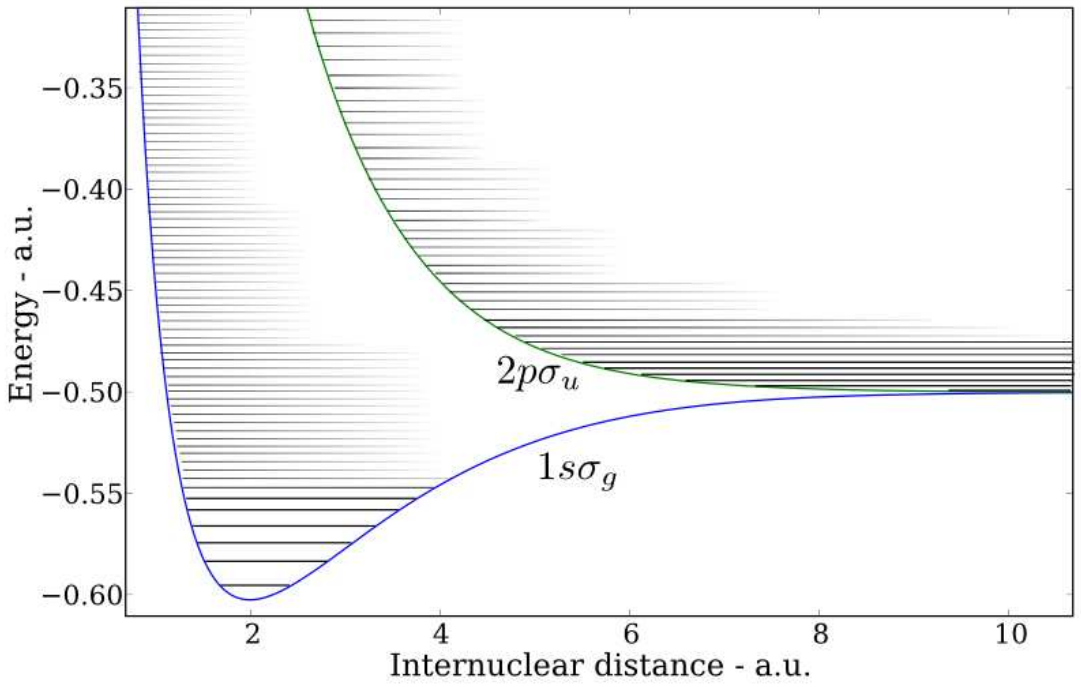

Figure 3.4: The vibrational energy levels, corresponding to the two lowest electric energy curves, $1s\sigma_g$ and $2p\sigma_u$.

For each electronic state, $\psi_e^i(\vec{x}; R)$, there is a set of vibrational states, $\chi_m^i(R)$, $m = 0, 1, 2....$ The energy levels of the vibrational states are scetched in Figure 3.4. The levels in the figure shows the total energy, which is shared by the electron, whose energy is given by the electric energy curve, and the nuclei, who get the energy difference between the curve and the total. The states with energy below the asymtotical value of the electronic energy curve are bound states, (e.g. the 15-20 lowest $1s\sigma_g$ states in the Fig. 3.4). If the energy is higher than this value, the states are dissosiative, or ionising, depending on the electronic energy. If the rotational energy were included in the calculation, there would in addition be a set of rotational states for each vibrational state.

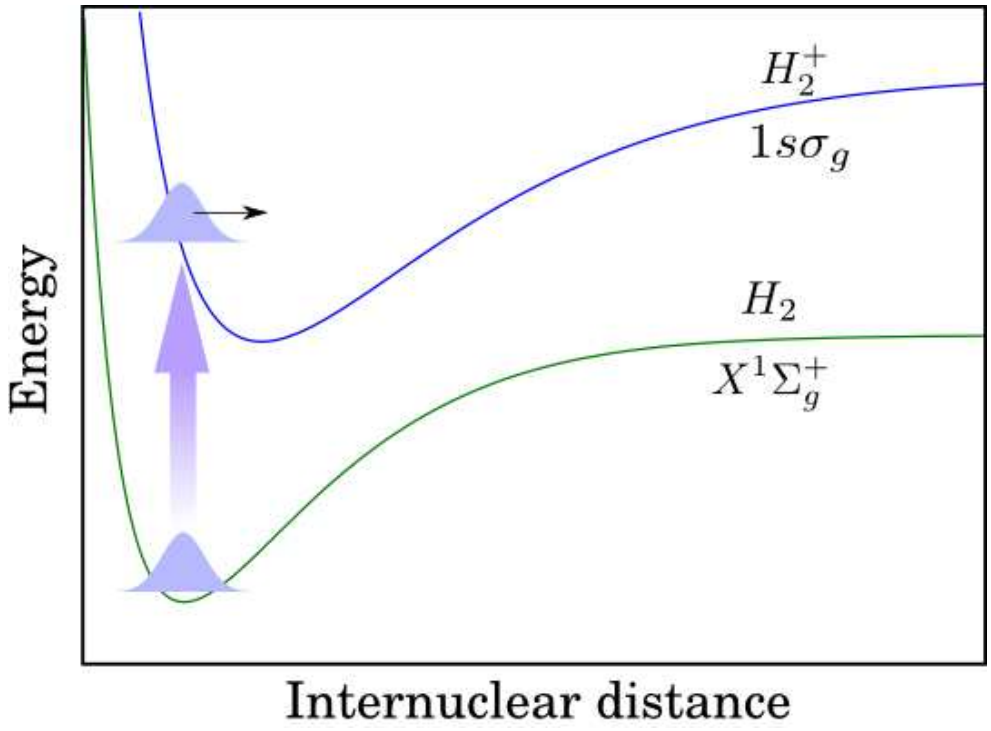

Figure 3.5: Franck-Condon transition from the ground state in H_2 to a superposition of states in H_2^+. Since the resulting wavepacket is not an eigenstate, it will propagate back and forth. The electronic energy curves are not to scale.

It is possible to prepare H_2^+ in the vibrational ground state in experiments [24], but typically in experiments [9], the laser pulse will ionise neutral H_2 molecules in hydrogen gas. One electron will be ionised first. The nuclear wavefunction, which used to be in the ground state of H_2, is no longer an eigenstate, since the system and its Hamiltonian has changed. Instead, the wavefunction is transfered to a superposition of the H_2^+ eigenstates, see Figure 3.5, according to the Franck-Condon (FC) principle [25], which states that a vibrational transition is more likely to occur if the final state overlaps with the initial state. If the transition is more or less instantaneous, the wavefunction, see Figure 3.6, will mostly retain its shape and position in the new system. A common approximation in the BO picture is to assume that the initial state in H_2^+ is the vibrational ground state of H_2. Since the Franck-Condon state, χ_{FC}, is not an eigenstate of H_2^+, it is written as a sum of the vibrational states of $1s\sigma_g$,

$$\chi_0^{X^1\Sigma_g^+} = \chi_{FC} = \sum_m c_m \chi_m^{1s\sigma_g} \tag{3.8}$$

The function is plotted in Fig. 3.6, for t = 0. If the function is propagated in time, it will

move to the right for ∼8 fs, and then move back to to the left. The new system will in turn interact with the laser, maybe resulting in dissosiation or full ionisation.

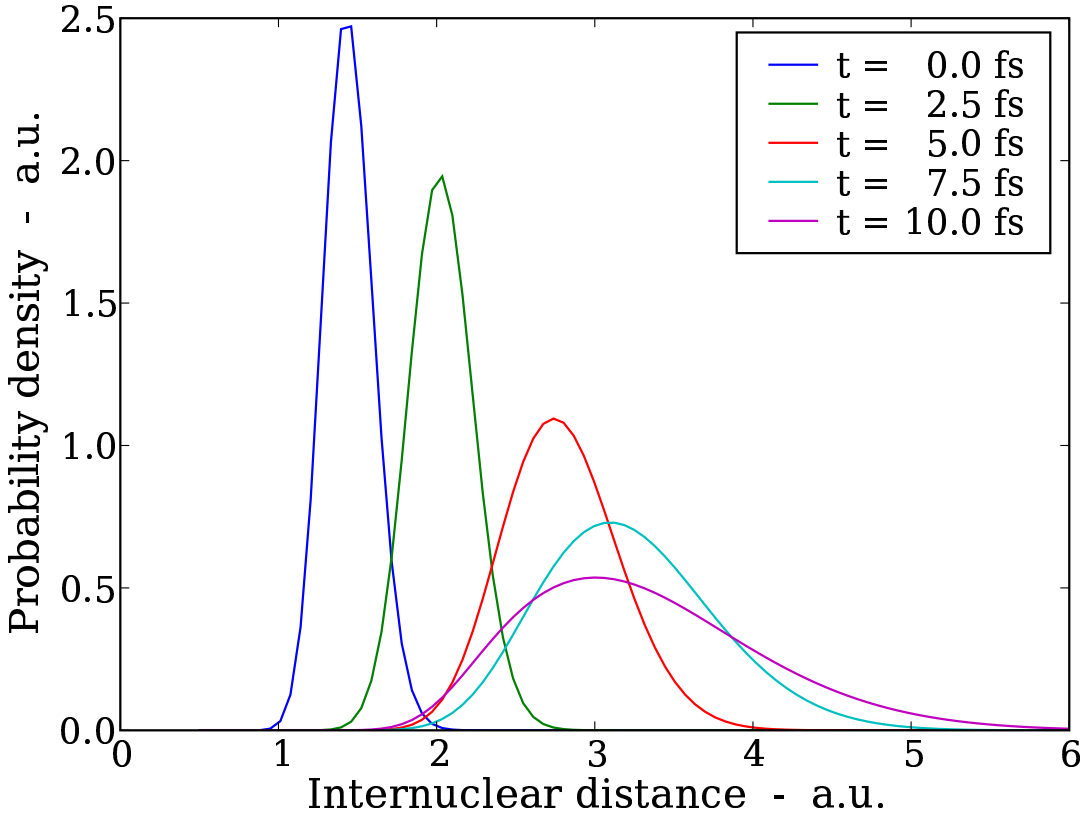

Figure 3.6: The $X^1\Sigma_g^+$ state of H_2 expanded in the vibrational states of $1s\sigma_g$ in H_2^+. Since the wavepacket is not an eigenstate, with time it will propagate back and forth.

The energy of the molecule fragments will be measured in detectors. After measuring enough particles, one gets a kinetic energy spectrum, i.e. a probability distribution in kinetic energy. When modelling this theoretically, the energy spectra must be calculated for comparison. The result of the calculation is simply a wavefunction, and it must be projected onto states with known energies. If the wavefunction is already expressed as a linear combination of known states, as in this thesis, the spectrum can be extracted with ease.

Chapter 4

A 1D model of H_2^+

Modelling H_2^+ in three dimensions is an enormous job. A three body problem in 3D makes nine dimensions. Three of these are ignored, since the problem is studied in the centre of mass reference frame. Further two nuclear dimensions can be dropped if the nuclei are not allowed to rotate. But four dimensions is quite a lot. If, for instance, an average of $N = 60$ basis functions are needed in each dimension, the total wavefunction will be a superposition of $N^4 \sim 10^7$ basis functions, and as a consequence, the Hamiltonian matrix contains a staggering $N^8 = 10^{14}$ elements. Though most of the elements will be zero, constructing this matrix, and time propagating the wavefunctions with it, demands serious time and computer power. A few simulations have been run in 3D, e.g. [26, 27, 28, 29, 15], but it is also common to reduce the problem to one dimension, [9, 10, 11, 12, 13, 14]. In 1D, the problem can be described using only two spatial dimensions, and the number of basis functions is reduced to N^2. This is more manageable, and allows one to run the simulations on larger domains. 1D models are widely used, partly because a lot of problems are to complex to be calculated in 3D yet. 1D simulations have to be done with caution, though. Much information is lost when discarding two dimensions, and one cannot expect the results to be the same as those found in experiments or 3D simulations. In this thesis we will introduce a more realistic 1D model. How this is done will be described in Section 4.2.

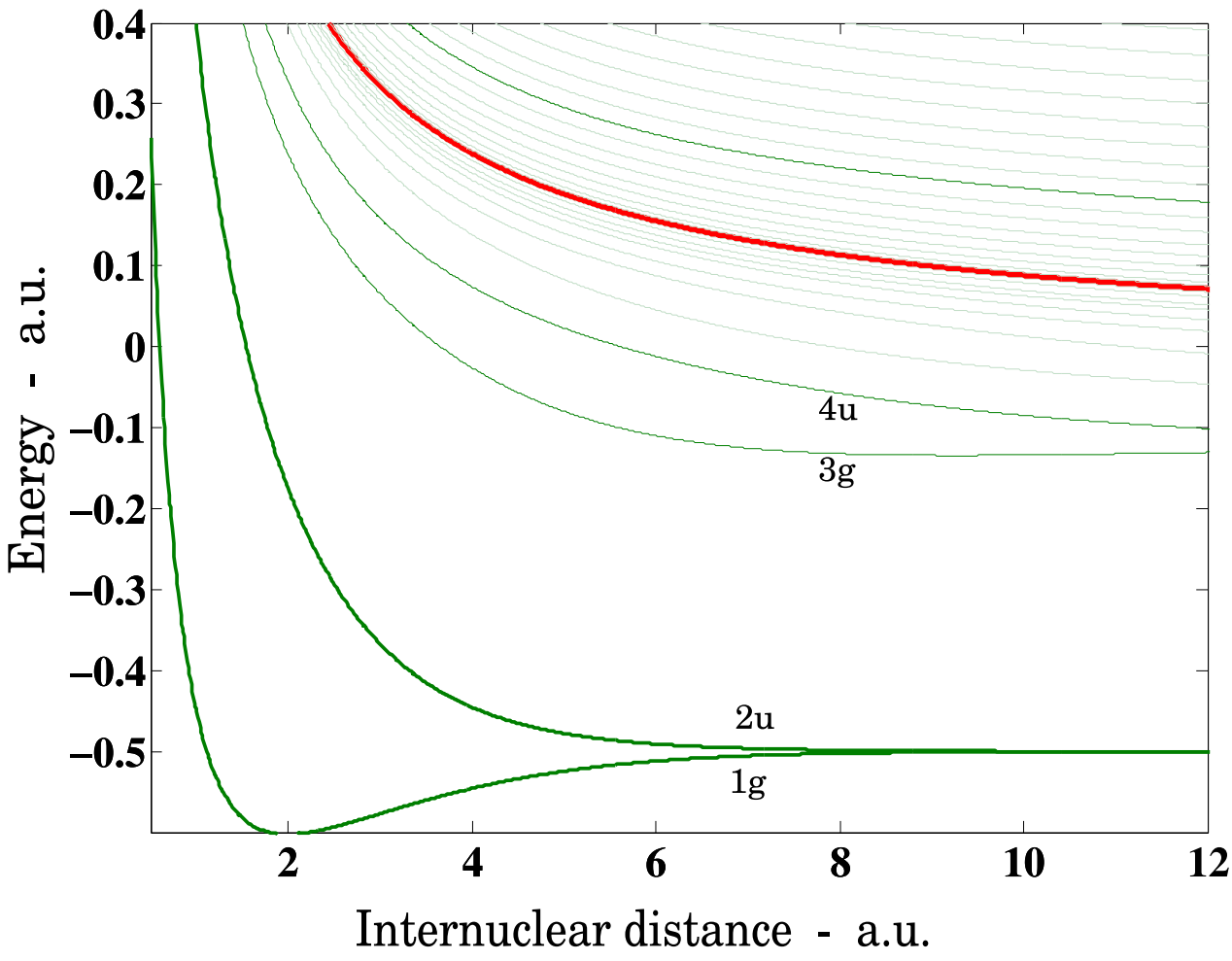

Figure 4.1: Electronic energy curves in the one dimensional H_2^+. Since there is no angular momentum in 1D, the curves are given names simply based on their energy and their symmetry.

The energy curves in 1D, drawn in Fig. 4.1, are given new names, as keeping the names from the 3D model would be misleading. The references to the angular momentum of the state are removed, and the names are given simply as a principal quantum number and a symmetry, i.e. $1g$, $2u$, $3g$,$4u$, etc.

We ran the H_2^+ simulation for several different scenarios. From the few 3D simulations on H_2^+ in the Born-Oppenheimer approximation, e.g. [30, 31, 32, 15, 16], we chose to look

at some of the interesting cases reported. This allowed us to test our model against real 3D calculations. We were also able to test if there were discrepansies between our BO calculations, and our non-BO calculations. In an article by Palacios *et al.*, called *Two-photon ionization of H_2^+ by short laser pulses* [15], structures in the energy spectrum were reported. The structures could, to a large extent, be reproduced in the one dimensional model. The model was also able to qualitatively recreate the work of Førre *et al.* in *Nuclear Interference in the Coulomb Explosion of H_2^+ in Short vuv Laser Fields* [16], where interference effects in the vibrational states led to characteristic structures in the dissosiation and ionisation energy spectra. We ran the scenarios with and without the BO approximation, which allowed us to look for discrepancies in the results.

The laser/molecule dynamics were done using the eigenstates of H_2^+ in the BO approximation as basis functions. The terms that were neglected when applying the BO approximation were reintroduced as a perturbation to $\widehat{H}$, and comparisons were done between results before and after these couplings were included in the Hamiltonian matrix. To find the basis functions, the TISE for H_2^+ was solved in the BO approximation, using a B-spline basis. The next chapters describe priciples and theory needed for doing the calculations of this thesis. Some focus will also be put on the implementation of the programs and the numerical considerations therein, before the simulations and resuls are discussed in detail in the last chapters.

4.1 The TISE in 1D

The Hamiltonian operator of H_2^+, Eq.(2.7), when directly translated into a one dimensional operator, takes the form

$$\widehat{H} = -\frac{\hbar^2}{2m_e}\frac{\partial^2}{\partial x^2} - \frac{\hbar^2}{2\mu}\frac{\partial^2}{\partial R^2} - \frac{ke^2}{\left|x+\frac{R}{2}\right|} - \frac{ke^2}{\left|x-\frac{R}{2}\right|} + \frac{ke^2}{|R|} \tag{4.1}$$

Applying the BO approximation to this problem goes exactly as for the 3D Hamiltonian. The position vectors are replaced by scalar values, as the three dimensional space has been replaced by the x-axis. The problem separates into two simpler problems like shown in Section 3.1. The electronic wavefunction, $\psi_e(x;R)$, is found by solving

$$\widehat{H}_e\psi_e(x;R) = E_e(R)\psi_e(x;R) \tag{4.2}$$

where the electronic Hamiltonian is

$$\widehat{H}_e = -\frac{\hbar^2}{2m_e}\frac{\partial^2}{\partial x^2} - \frac{ke^2}{\left|x+\frac{R}{2}\right|} - \frac{ke^2}{\left|x-\frac{R}{2}\right|} \tag{4.3}$$

The vibrational wavefunction, $\chi(R)$, is found by solving

$$\left[-\frac{\hbar^2}{M}\frac{\partial^2}{\partial R^2} + E_e(R) + \frac{ke^2}{|R|}\right]\chi(R) = E\chi(R) \tag{4.4}$$

4.2 Adjusting the 1D Coulomb potential

When using a one dimensional model of a three dimensional problem, certain adjustments have to be made. Upon comparison with the 3D model, results gathered from the 1D model will provide qualitative agreement at best. However, for comparison to be even possible, changes need to be made in the Hamiltonian. The singularity in the Coulomb potential will be a lot more dominating in 1D than in 3D. If one pictures the electron as a particle moving around the nuclei, it is easy to see that while the electron can circle each nucleus any which way in three dimensions, in one dimension it is forced to go *through* the nuclei. To make the system resemble the three dimensional representation, one includes *softening* parametres, σ, to the potential. The Coulomb terms in the H_2^+ Hamiltonian then changes from

$$V_{Coulomb} = -\frac{ke^2}{\left|x+\frac{R}{2}\right|} - \frac{ke^2}{\left|x-\frac{R}{2}\right|} + \frac{ke^2}{|R|} \tag{4.5}$$

to

$$V_{Coulomb} = -\frac{ke^2\sigma_1}{\sqrt{\left(x+\frac{R}{2}\right)^2+\sigma_2}} - \frac{ke^2\sigma_1}{\sqrt{\left(x-\frac{R}{2}\right)^2+\sigma_2}} + \frac{ke^2}{|R|} \tag{4.6}$$

This is called a regularised Coulomb problem. Values for σ_1 and σ_2 were chosen to make the electronic energy curves, $E_e(R)$, mimic the three dimensional case as closely as possible.

At this point we went further than what is common. The two lowest curves, corresponding to the ground state, $1g$, and the first excited state, $2u$, are of special interest in this work. These were fitted to the real 3D-energies, $1s\sigma_g$ and $2p\sigma_u$, as closely as possible, by allowing σ_2 to become R-dependent, (see Fig. 4.2),

$$\sigma_2 \quad \rightarrow \quad \sigma_2(R)$$

This is a new approach, making the 1D model more comparable to the 3D model. The optimalisation was done by making a function in Python [33], $f(\sigma_2)$, that solved the electronic Schrödinger equation for the given σ_2, and returned the difference between the calculated ground state energy and the real H_2^+ ground state energy [34].

$$f(\sigma_2) \quad = \quad E_1^{1D} - E_1^{3D}$$

A least square method in the Python library[1] found σ_2 values for a sufficient number of points on the R-axis. The $2u$ curve does not match ideally for $R < 2$ a.u., but for larger R, in the area of interest in this work, the conformity is good. (See Table 4.1.) Allowing the softening parametre to change with the internuclear distance is a new approach. The conventional modus operandi is to keep $\sigma_2(R) \equiv 2$, or some nearby constant. Figure 4.3 shows the resulting $1g$ and $2u$ electronic energy surfaces. The solid lines are our adapted curves. They are almost the same as the 3D curves, who for that reason is not included in the figure. One sees the marked difference between our curves and the curves constructed with constant softening parametres. The common choice, $\sigma_2 = 2$ a.u., puts the minimum in $1g$ at $\sim$1.4 a.u. right of the correct placement.

[1] scipy.optimize.leastsq()

Table 4.1: The table shows the values used for $\sigma_2(R)$, and the resulting energy curves. The 3D energy curves [34], are included for comparison.

R	σ_2	$1g$ Model energies	$1s\sigma_g$ Real energies	$2u$ Model energies	$2p\sigma_u$ Real energies
(a.u.)	(a.u.)	(a.u.)	(a.u.)	(a.u.)	(a.u.)
1.0	0.1931550	-0.4518004	-0.4517863	0.3935613	0.4351863
2.0	0.2508971	-0.6026424	-0.6026342	-0.1762692	-0.1675344
3.0	0.2863316	-0.5775650	-0.5775629	-0.3682164	-0.3680850
4.0	0.3123320	-0.5460855	-0.5460849	-0.4457946	-0.4455064
5.0	0.3339039	-0.5244203	-0.5244203	-0.4777170	-0.4772916
6.0	0.3517653	-0.5119695	-0.5119690	-0.4908747	-0.4906439
7.0	0.3661765	-0.5055945	-0.5055940	-0.4963323	-0.4962717
8.0	0.3777629	-0.5025707	-0.5025704	-0.4985972	-0.4986060
9.0	0.3872043	-0.5011956	-0.5011954	-0.4995214	-0.4995438
10.0	0.3950349	-0.5005788	-0.5005787	-0.4998833	-0.4999011
11.0	0.4016353	-0.5002994	-0.5002992	-0.5000136	-0.5000244
12.0	0.4072751	-0.5001684	-0.5001683	-0.5000521	-0.5000579
13.0	0.4121492	-0.5001036	-0.5001035	-0.5000566	-0.5000595
14.0	0.4164029	-0.5000690	-0.5000689	-0.5000501	-0.5000515
15.0	0.4201464	-0.5000490	-0.5000489	-0.5000415	-0.5000421
16.0	0.4234661	-0.5000364	-0.5000364	-0.5000335	-0.5000337
17.0	0.4264297	-0.5000280	-0.5000279	-0.5000268	-0.5000269
18.0	0.4290913	-0.5000220	-0.5000220	-0.5000215	-0.5000216
19.0	0.4314946	-0.5000176	-0.5000176	-0.5000174	-0.5000174
20.0	0.4336752	-0.5000143	-0.5000143	-0.5000142	-0.5000142
21.0	0.4356629	-0.5000117	-0.5000117	-0.5000117	-0.5000117
22.0	0.4374819	-0.5000097	-0.5000097	-0.5000097	-0.5000097
23.0	0.4391529	-0.5000081	-0.5000081	-0.5000081	-0.5000081
24.0	0.4406930	-0.5000069	-0.5000068	-0.5000069	-0.5000068
25.0	0.4421171	-0.5000058	-0.5000058	-0.5000058	-0.5000058

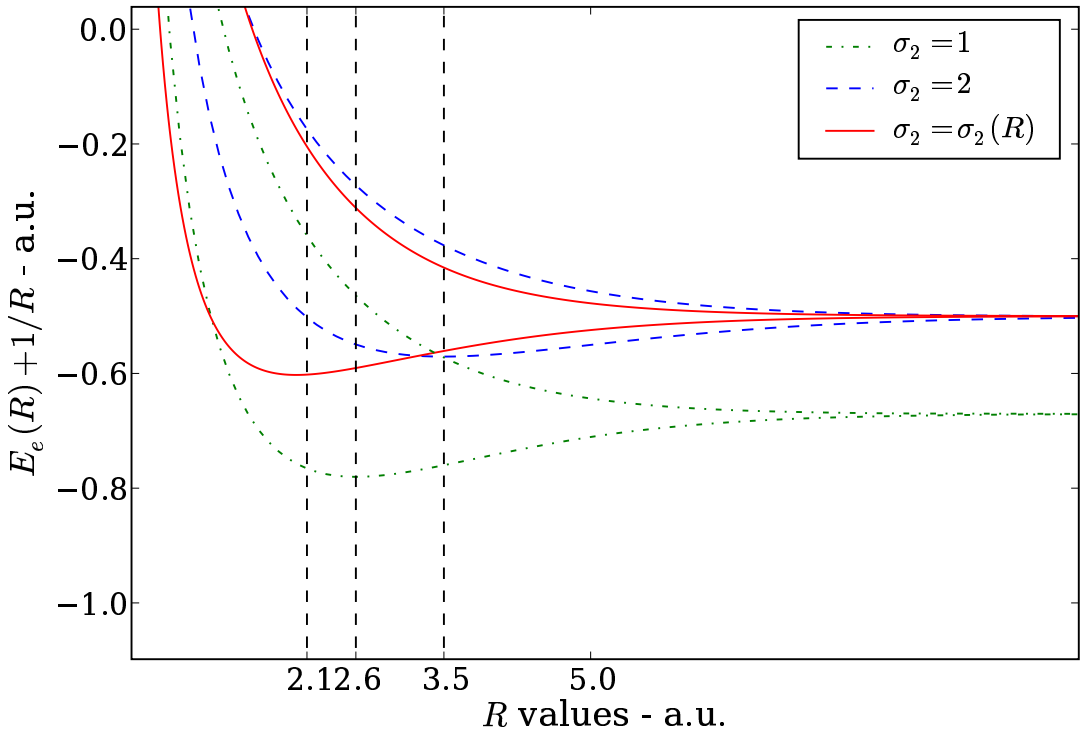

Figure 4.3: The two lowest energy curves, using different softening parametres. The curves with an R dependent parametre (solid) are more or less identical to the 3D curves, and the ground state has a minimum at $R_0 = 2.1$ a.u. When σ_2 was kept constant at 2 (dashed), as used in [27], the shape of the curves deviates markedly, ($R_0 = 3.5$ a.u.), whereas with $\sigma_2 = 1$, (dash-dot), as used in [9], the shape is somewhat better, ($R_0 = 2.6$ a.u.), but the energies are lower. The dashed vertical lines show the minima of the ground state curves.

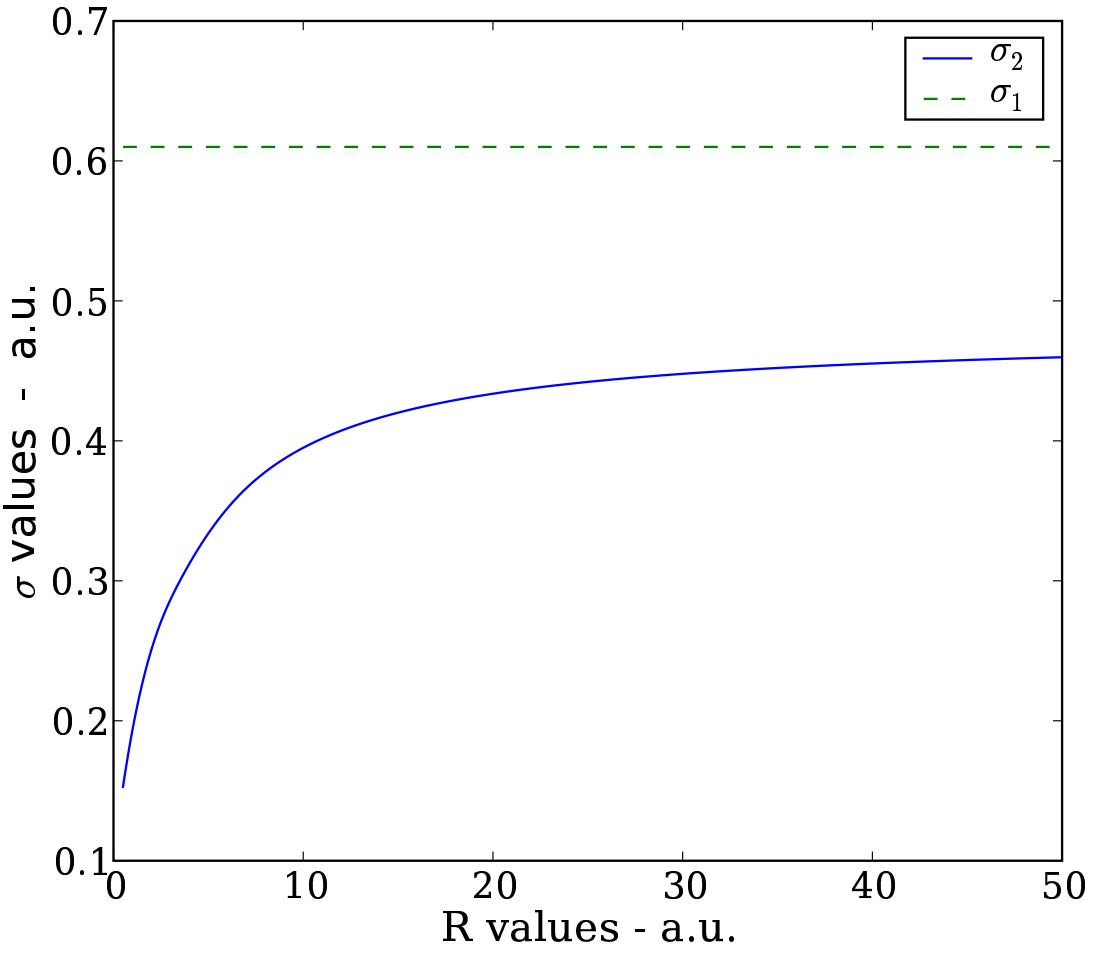

Figure 4.2: The softening parametres, σ_1 and σ_2, that reproduced the two lowest energy curves in H_2^+. $\sigma_1 = 0.61$ was constant for all R, whereas $\sigma_2(R)$ was allowed to change.

Chapter 5

Wavefunction expansion and basis functions

5.1 Wavefunction expansion

One of the important tools in a quantum mechanic's toolbox, is the wavefunction expansion. Any function can be written as a sum of other known functions,

$$f(x) = \sum_{i=1}^{\infty} c_i g_i(x), \qquad \{g_i(x)\}, \quad \text{set of basis functions} \tag{5.1}$$

where $g_i(x)$ is the ith of these known functions, from now on called *basis functions*, and c_i is the weight of the ith function in the sum. Well known examples of this is the Taylor expansion, where the basis functions are polynomials, and the Fourier expansion, where the basis functions are sine and cosine functions. In fact, any set of basis functions that form a *complete set*[1], (i.e. the basis functions span out the entire function space) can be used.

In numerical applications, it is impractical to use a sum that goes to infinity, so one sums only over a finite number, N, of basis functions,

$$f(x) = \sum_{i=1}^{\infty} c_i g_i(x) \rightarrow f(x) \approx \sum_{i=1}^{N} c_i g_i(x) \tag{5.2}$$

This introduces a truncation error. However, for a reasonable basis set, the coefficients, c_i, will drop toward zero when i increases. If N is sufficiently large, the contributions from

[1] For more details on this, see [35].

the ($i > N$) terms are negligible. If the wavefunction is expanded in basis functions, the time independent Schrödinger equation takes the form

$$\widehat{H}\Psi = E\Psi$$
$$\widehat{H}\sum_{i=1}^{N} c_i g_i = E\sum_{i=1}^{N} c_i g_i$$

where $\widehat{H}$ is the Hamiltonian operator, Ψ is the wavefunction, E is the energy and g_i is the ith basis function. To find Ψ, one needs to determine the coefficients, c_i.

The complex conjugated of a basis function is multiplied with the equation from the left, one integrates over space, and one gets a linear equation with $N + 1$ unknowns.

$$\sum_{i=1}^{N} c_i \int g_j^* \widehat{H} g_i = E\sum_{i=1}^{N} c_i \int g_j^* g_i$$

This is done for all the N basis funtions[2], and one ends up with a system of linear equations, that can be written on the form,

$$H\vec{c} = SE\vec{c} \tag{5.3}$$

The coefficients, c_i, are written as a vector, $\vec{c}$. The Hamiltonian operator has been replaced by a $N \times N$ Hamiltonian matrix, H. Each matrix element is given as

$$H_{j,i} = \int g_j^* \widehat{H} g_i, \qquad \text{in bra-ket notation: } \langle g_j | \, \widehat{H} \, | g_i \rangle \tag{5.4}$$

On the right hand side in Eq. (5.3), one gets the slightly simpler matrix, called the *Overlap matrix*, S, with matrix elements

$$S_{j,i} = \int g_j^* g_i, \qquad \text{in bra-ket notation: } \langle g_j \mid g_i \rangle \tag{5.5}$$

Solving the Schrödinger equation has now been reduced to the linear algebra problem of finding $\vec{c}$ and E.

5.2 Choosing a basis

The basis functions determine how the matrices will end up. One basis set may need a lot more basis functions to approximate a function well than another. The function expansion

[2] N equations, and $N + 1$ unknowns. How does that add up? An extra equation appear in our normalisation demand, $\langle \Psi \mid \Psi \rangle = 1$.

is acceptable when

$$\left\| \sum_{i=1}^{N} c_i g_i - f \right\| < \varepsilon \tag{5.6}$$

where g_i are the functions in our basis set, f is the function to be expanded and ε is the given tolerance. We want to choose a basis set that makes N small, since N is the dimensions of the H and S matrix. It is common to choose an orthogonal basis. In that case

$$\int g_j^* g_i = \langle g_j \mid g_i \rangle = A\delta_{i,j} \tag{5.7}$$

where $\delta_{i,j}$ is the Kronecker delta function

$$\delta_{i,j} = \left.\begin{array}{ll} 1, & i = j \\ 0, & i \neq j \end{array}\right\} \tag{5.8}$$

This simplifies the linear algebra problem considerably, as the S matrix will become diagonal. For convenience, the basis can be made ortonormal, i.e. the A from (5.7) is 1. Then the overlap matrix will simply become the identity matrix. In quantum mechanics, the basis functions may be chosen to be solutions of the Schrödinger equation for a related problem. For instance, if $\widehat{H}$ resembles a harmonic oscillator, the analytically known solutions to the harmonic oscillator potential, namely the Hermite polynomials, is an appropriate basis set [36].

When solving the time independent Schrödinger equation for H_2^+ in this undertaking, a B-spline basis is used. The B-splines are not orthogonal, but a property of the basis is that H and S will be banded matrices, which are easier to diagonalise. In addition, a B-spline expansion can approximate most functions efficiently.

When performing laser/molecule dynamics, the solutions of the TISE for H_2^+ in the BO approximation are used as a basis. It is an orthogonal basis set, easy to truncate, and very good for interpreting the results.

5.3 B-splines

The basis functions in a B-spline basis set are piecewise polynomials [37], splined into a bell shaped curve as can be seen in Fig. 5.1.

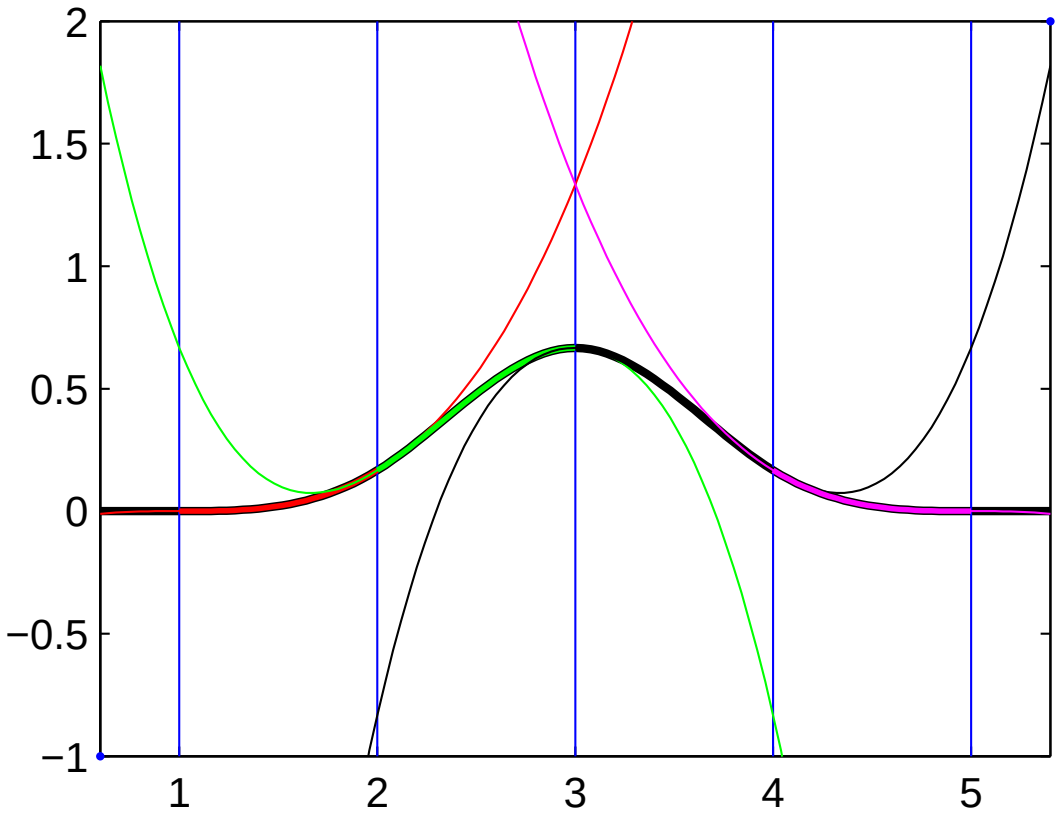

Figure 5.1: The B-spline function (bold line) is a piecewise polynomial. The polynomial constituents (thin lines) contribute to the final curve on an interval each. The intervals are separated by *knotpoints*, shown here as vertical lines. This B-spline is of order 4, i.e. it is nonzero over four intervals, and is made up of third order polynomials. The knotpoints are {1,2,3,4,5}.
The figure was made using a function from the Matlab library, *bspline()*.

Typically, the next function in the basis will be identical, but shifted a knotpoint interval to the right. When defining a B-spline basis for a domain $[a, b] \in \mathbb{R}$, one first defines a sequence of *knotpoints*. Each knotpoint marks the beginning of a B-spline[3]. If the function to be approximated is oscillating or changing rapidly, the knotpoints must be closely spaced. For nicely behaving functions, they can be further apart. The knotpoints need NOT be equidistant. Herein lies one of the advantages of the B-spline basis. For the swiftly oscillating portions of the function, a dense grid of knotpoints may be used, and for the moderate parts, a wider spacing will do nicely. One then has to choose the

[3]Except for the last k knotpoints, which only mark the ending of the splines, (k being the order of the B-splines).

order, k, of the B-splines. Each spline function will stretch over k intervals, an interval being the space between neighbouring knotpoints. The function is made up of a different polynomial (of order $k-1$) on each interval, smoothly[4] joined at the knotpoints. Outside of these intervals, the function is 0. This means that on any point on the domain there will be exactly k nonzero splines. High enough order is important for making a good function approximation. In quantum mechanical applications, k is typically chosen to be between 6 and 9 [38].

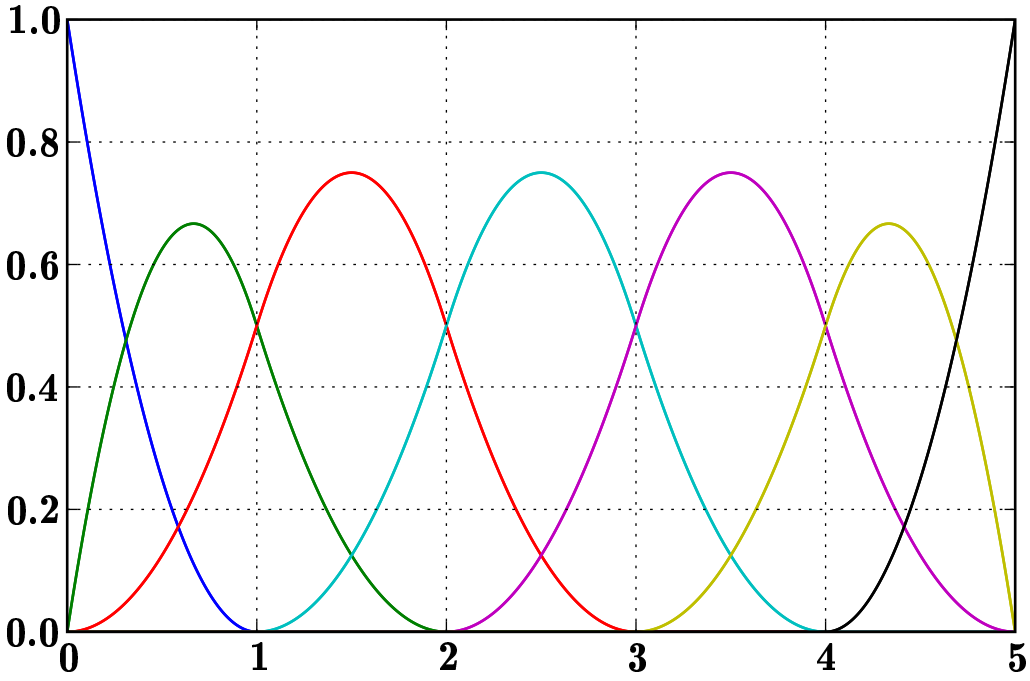

Figure 5.2: The entire B-spline basis, of order $k = 3$, for the knotsequence {0, 0, 0, 1, 2, 3, 4, 5, 5, 5}. The sum of all the functions will be 1 everywhere on the domain [38].

The B-spline basis functions are defined by the recursion formula

$$B_i^k(x) = \frac{x - t_i}{t_{i+k-1} - t_i} B_i^{k-1}(x) + \frac{t_{i+k} - x}{t_{i+k} - t_{i+1}} B_{i+1}^{k-1}(x) \tag{5.9}$$

$$B_i^1(x) = \left.\begin{array}{ll} 1, & t_i \leq x < t_{i+1} \\ 0, & \text{otherwise} \end{array}\right\} \tag{5.10}$$

[4] In the interior of the domain, the continuity is typically C^{k-2}. The continuity at the edges of the domain is of lower order. The first and last splines will not even be continuous.

where B_i^k is the ith basis function, k is the order and t_i is the ith knotpoint, i.e. the starting point of the ith spline, (or the end point of the $(i-k)$th spline). As one can see from Equation (5.10), the first order B-spline is a step function, that is one on its interval, and zero everywhere else.
The derivatives of a B-spline function may be found by the recursion relation,

$$DB_i^k(x) = \frac{k-1}{t_{i+k-1} - t_i} B_i^{k-1}(x) - \frac{k-1}{t_{i+k} - t_{i+1}} B_{i+1}^{k-1}(x) \tag{5.11}$$

The derivatives are necessary when calculating the Hamiltonian matrix elements.

If one were to use the recursion formula every time a spline value was needed, from a numerical point of view, it would soon become cumbersome. As it turns out, one only need the B-spline values from the same set of points for most operations, and these can be saved to a table, and quickly called up when needed.
The spline values will mostly be needed for calculating integrals on the domain. To perform these integrals, a Gauss Legandre quadrature formula[5] is used.

$$I = \sum_{i=1}^{N} w_i f(x_i) \tag{5.12}$$

The integral, I, is reduced to a sum with N terms, of the integrand, $f(x)$, evaluated in *specific* nodes, x_i, weighted with w_i. x_i and w_i can readily be calculated [39, p 304]. This integration is exact for polynomials up to a degree $2N-1$. The B-splines are piecewise polynomials, and the integrand is typically a product of two B-splines, i.e. a piecewise polynomial of order $2k-2$. On each interval, the integral can be found exactly with only k function evaluations[6].

The total number of B-spline evaluations needed, will then be $2N_B k^2$, where N_B is the total number of B-splines. Each of these will stretch over k intervals, and each interval needs k function evaluations. The factor 2 comes from also calculating the derivative of the B-splines, which is needed for the kinetic energy part of the Hamiltonian.

[5] For more on Gaussian quadrature, see [39, pp 301-307].

[6] This obviously holds when calculating Equation (5.5), but what of Eq. (5.4)? The integrand will not necessarily be a simple polynomial. Experience has shown, though, that for any $\widehat{H}$ in this work, the integral can be evaluated to machine precicion using only k nodes.

5.4 TISE eigenfunction basis

When the Hamiltonian is on the form

$$\widehat{H} = \widehat{H}_0 + \widehat{H}',$$

where $\widehat{H}_0$ is easier to solve than the full problem, ($\widehat{H}'$ may for instance be time-dependent), it is common to solve the TISE for $\widehat{H}_0$, and use the solutions as a basis for solving the full problem. The Hamiltonian is hermitian [1, p 23], i.e. the eigenvalues (energies) are real, and its eigenfunctions are orthogonal [40, p 233]. When constructing the full Hamiltonian matrix, using the wavefunctions, $|\psi_i\rangle$, from $\widehat{H}_0$ as a basis, there will not be an overlap matrix. The additional benefit is that only the interaction with $\widehat{H}'$ needs to be calculated, as can be seen when the matrix elements are written explicitly,

$$\begin{aligned} H_{i,j} &= \langle\psi_i| \widehat{H}_0 + \widehat{H}' |\psi_j\rangle \\ &= \langle\psi_i| E_j |\psi_j\rangle + \langle\psi_i| \widehat{H}' |\psi_j\rangle \\ &= E_j\delta_{ij} + \langle\psi_i| \widehat{H}' |\psi_j\rangle \end{aligned}$$

The contribution from $\widehat{H}_0$ will be the eigenstate energies, E_i, on the matrix diagonal.

Provided that $\widehat{H}'$ is not too big, the eigenfunctions of $\widehat{H}_0$ should be able to approximating the wavefunction using relatively few basis functions. However, the real advantages of using the eigenfunction basis is in interpreting the result, and the possibility of truncating the basis set to keep only the essensial states, i.e. the states that one can expect to be populated. The vector attained when solving the TDSE contains the amplitudes of the basis functions. For the physical analysis, it is preferable to have the result as a linear combination of actual physical wavefunctions, with known energies, rather than mathematical functions, such as in the B-spline basis.

Chapter 6

The numerical calculation of the TISE and the TDSE

6.1 Implementing the TISE solver

The software made for this thesis is almost completely Python code, with some Fortran90 mixed in to do the heavy lifting. The entire source code is availabe at [41]. A 1D TISE solver, (based on a program by Raymond Nepstad), was the starting point of the programming. It creates a B-spline basis for the problem, constructs the Hamiltonian in that basis, and solves the eigenvalue problem. The user interface is a config file, where one can supply the specifications: particle mass, potential, domain, number and order of B-splines and knotpoint distribution. The B-spline values are tabulated in the integration points and saved, and the Gauss Legendre integration method use these tables.

The TISE solver was used on the two linked differential equations describing the molecule. When the softening parametres are included, the electronic wave equation takes the form

$$\left[-\frac{1}{2}\frac{\partial^2}{\partial x^2} - \frac{\sigma_1}{\sqrt{\left(x+\frac{R}{2}\right)^2+\sigma_2}} - \frac{\sigma_1}{\sqrt{\left(x-\frac{R}{2}\right)^2+\sigma_2}}\right]\psi_e(\vec{r};\vec{R}) = E_e(R)\psi_e(\vec{r};\vec{R}) \tag{6.1}$$

For convenience, atomic units have been introduced, meaning $\hbar = 1$ a.u., $m_e = 1$ a.u. and $e = 1$ a.u. Atomic units are used exclusively in the rest of the thesis. The operator for the vibrational motion of the nuclei includes the solutions of Eq. (6.1),

$$\left[-\frac{1}{M}\frac{\partial^2}{\partial R^2} + E_e(R) + \frac{1}{|R|}\right]\chi(\vec{R}) = E\chi(\vec{R}) \tag{6.2}$$

Because the potential energy curves, $E_e(R)$, are needed to solve Eq. (6.2), Eq. (6.1) must be solved first. It also follows that it needs to be solved for enough values of R, so that the curves $E_e(R)$ can be resolved sufficiently to solve Eq. (6.2). The matrix elements of the vibrational Hamiltonian are integrals over the R domain, calculated with quadrature formulae. To satisfy any reasonable demands of accuracy, $E_e(R)$ was found in all the integration points in R.

Solving Eq. (6.1) and Eq. (6.2) gives us the electronic wavefunction, $\psi_e(x;R)$, the vibrational wavefunction, $\chi(R)$, the electronic energies, $E_e(R)$ and the total energies, E. When the wavefunctions are calculated from the diagonalisation, their signs are arbitrary. This is a problem when calculating the electronic wavefunctions for different R independently. There is no guaranty the wavefunction for one R will have the same sign as its neighbour. The signs of the wavefunctions therefore had to be set manually, to make sure it stayed the same throughout. Since the wavefunctions changes with R, albeit slowly, one cannot simply choose an x value, and demand that the sign of the wavefunction at that x-value stays constant. A safe way to do it is to find the maximum of the wavefunction, and making sure the sign is the same in that point for the next R value. This was done for each wavefunction and each R. There will naturally be as many electronic energy curves as there are functions in the basis. Not all of them are physically valid, as will be discussed in Section 6.3. For each of the curves that are used, one needs to solve Eq. (6.2).

Summing up:

1. Create the B-spline basis for the R and x variable.

2. Solve Eq. (6.1) for all R on the integration grid, and save the energies and wave functions.

3. Solve Eq. (6.2) for the N lowest energy curves. (How to decide N will be shown later.) Save the energies and the wave functions.

6.2 Solving the time dependent Schrödinger equation for H_2^+

The results in this thesis were arrived at by solving the time dependent Schrödinger equation, (TDSE),

$$i\hbar\frac{\partial\Psi_{tot}(x,R)}{\partial t} = \widehat{H}(R,r,t)\Psi_{tot}(x,R)$$

where the wavefunction, expressed in the BO state basis reads

$$\Psi_{tot}(x,R) = \sum_i \sum_m c_{i_m}\psi_e(x;R)_i\chi(R)^i_m \tag{6.3}$$

For a given Hamiltonian, the system was propagated in time using an ODE solver. We used an old Fortran 77 code, based on the Adams - Moulton method [35]. It is a multistep method, i.e. it uses several of the previous function values for calculating the next step. The code uses a predictor-corrector formula. That means an explicit method is used initially, and the result is then corrected for each step using an implicit formula. The code is adaptive, meaning it changes the length of the time steps based on local error estimates. The full description of the algorithm can be read in [42]. The following sections describe how the Hamiltonian matrix was calculated.

6.2.1 The Hamiltonian matrix

The Hamiltonian for the whole problem can be written

$$\widehat{H}(x,R,t) = \widehat{H}_{BO}(x,R) + \widehat{H}_{laser}(x,t) + \widehat{H}_{NBO}(R) \tag{6.4}$$

The first part, $\widehat{H}_{BO}$, is the time independent Hamiltonian of H_2^+, in the BO approximation, written explicitly in Eq. (6.1) and Eq. (6.2). This problem was solved first, using a B-spline basis. The eigenfunctions that were attained, were used as basis functions for solving the full time dependent problem. The Hamiltonian of the laser field, $\widehat{H}_{laser}$, represents the energy from the electric field, (see section 2.3). In one dimension, and atomic units, it is simply

$$\widehat{H}_{laser} = E(t)x$$

The electric field strength, $E(t)$, describes the pulse, and will be different depending on which case is being studied. The last term in Eq. (6.4), $\widehat{H}_{NBO}$, contains the terms that

were neglected when introducing the BO approximation. Since it acts on only parts of the wavefunction, it cannot be written out properly as operators, but working on a BO basisfunction, it takes this form:

$$\begin{aligned}\widehat{H}_{NBO}\Psi_{tot}(x,R) &= \widehat{H}_{NBO}\psi_e(x;R)\chi(R) \\ &= -\frac{1}{M}\left(2\frac{\partial\psi_e(x;R)}{\partial R}\frac{\partial\chi(R)}{\partial R} + \chi(R)\frac{\partial^2\psi_e(x;R)}{\partial R^2}\right)\end{aligned}$$

The reintroduction of $\widehat{H}_{NBO}$ will remove the BO approximation error. Each matrix element in the full Hamiltonian will be calculated from the equation

$$H_{\eta,\xi} = \left\langle \Psi^{\eta}_{tot} \middle| \widehat{H}_{BO}(x,R) + \widehat{H}_{laser}(x,t) + \widehat{H}_{NBO}(R) \middle| \Psi^{\xi}_{tot} \right\rangle$$

The basis functions are ordered a certain way:

$$\begin{aligned} |\Psi^{\eta}_{tot}\rangle &= \left|\psi^i_e\chi^m_i\right\rangle \quad , \qquad \eta = i\cdot N_{vib} + m \\ \left|\Psi^{\xi}_{tot}\right\rangle &= \left|\psi^j_e\chi^n_j\right\rangle \quad , \qquad \xi = j\cdot N_{vib} + n \end{aligned}$$

$$i,j = 1,2,...,N_{el} \qquad m,n = 1,2,...,N_{vib} \qquad \eta,\xi = 1,2,...,N_{el}\cdot N_{vib}$$

where N_{el} is the number of electronic energy curves, and N_{vib} is the number of vibrational states for each curve. ψ^i_e is the ith electronic state, χ^m_i is the mth vibrational state of the ith potential curve. In other words, the basis is ordered with every state corresponding to the lowest energy curve first, in order of ascending energy, then every state corresponding to the first excited electronic curve, and so on.

6.2.2 The dipole couplings

The electric field of the laser contributes to the total Hamiltonian through $\widehat{H}_{laser}$. The matrix elements from this operator takes the form

$$\begin{aligned} H_{\eta,\xi} &= E(t)\left\langle \Psi^{\eta}_{tot}\,|x|\,\Psi^{\xi}_{tot}\right\rangle \\ &= E(t)\left\langle \chi^m_i \middle| \left\langle \psi^i_e\,|x|\,\psi^j_e\right\rangle_x \middle| \chi^n_j\right\rangle_R \end{aligned}$$

For the test scenarios described in Chapter 7 and Chapter 8, a basis set with $6\cdot 10^4$ basis functions was used. However, it is not necessary to calculate all the $3\cdot 10^9$ or so matrix elements this leads to. First of all, the Hamiltonian matrix is symmetric. That reduces the task to finding elements from the diagonal and up. Second, the electronic Hamiltonian, (Eq. (4.3)), commutes with the parity operator. Since the energy levels are not degenerate,

this means that the wavefunctions, $\psi_e(x;R)$, will have well defined parity, i.e. they will be even or odd [1, p 72]. As it turns out, with raising energy, every second is even, every second is odd. This makes some sense, as at each new energy level, the wavefunction gets another node, thereby flipping the parity. As a consequence of this,

$$\left\langle \psi_e^i \left| x \right| \psi_e^j \right\rangle = 0, \quad \text{when} \quad i+j \quad \text{is an even number.}$$

In these cases, the integrand will be odd, and as the domain is symmetrical around the origin, the integral will be zero. This means another factor 2 work reduction. One should of course notice that $\langle \psi_e^i \left| x \right| \psi_e^j \rangle$ needs only be calculated once for all the states corresponding to the electronic energy curves denoted by i and j. $\langle \psi_e^1 \left| x \right| \psi_e^2 \rangle$, i.e. the electronic coupling between $1g$ and $2u$, is plotted in Fig. 6.1. For comparison, the coupling between the $1s\sigma_g$ and $2p\sigma_u$ curves in the three dimensional model is plotted as well. The couplings are remarkably similar, which bodes well for the dynamics on these curves.

The program written to find the matrix elements first calculated all the electronic couplings. Despite the symmetries mentioned above, which meant there were only $\frac{N_{el}^2}{4}$ couplings needed, it is a huge job. The reason is that it must be calculated for several values of R on the integration grid, making each coupling a function of R.

$$f(R) = \left\langle \psi_e^i(x;R) \left| x \right| \psi_e^j(x;R) \right\rangle_x \tag{6.5}$$

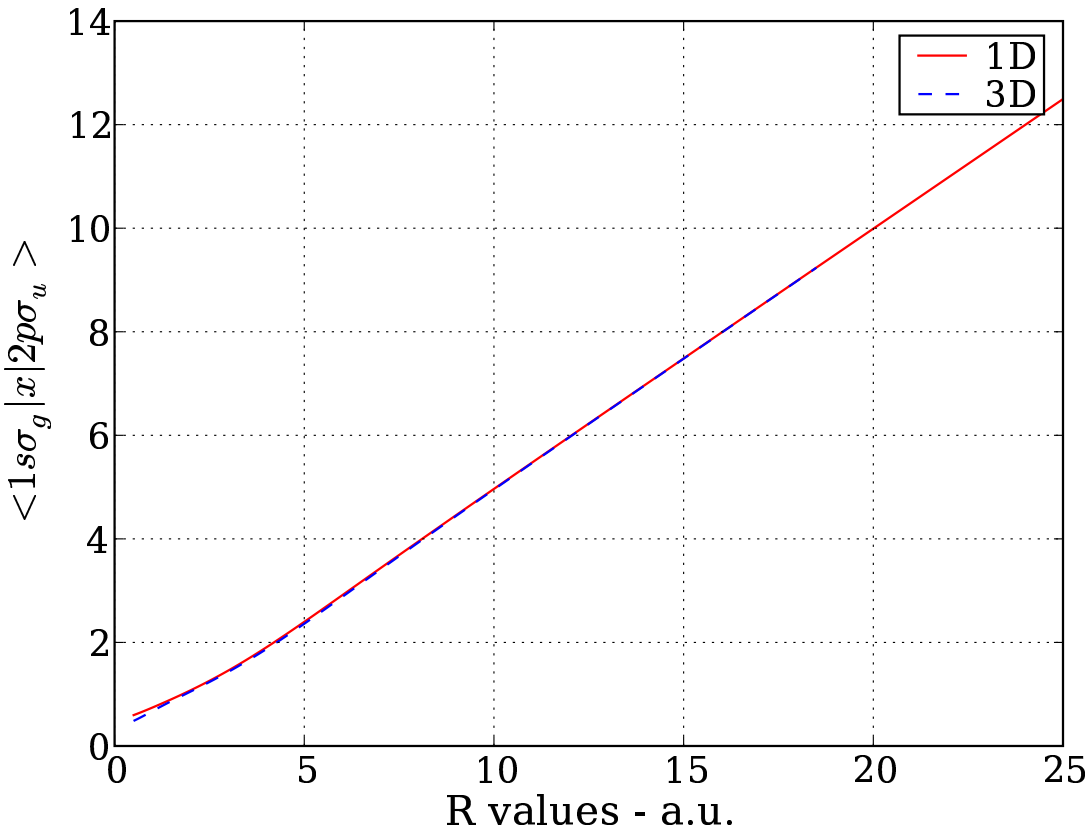

Figure 6.1: The dipole coupling between the two lowest energy curves, $1g$ and $2u$. The function goes approximately as $\frac{R}{2}$ when R is large. The dashed line is the coupling in the 3D model, and the solid line is the coupling in the 1D model.

When these were computed, one integrated over R,

$$\langle \chi^m \left| f(R) \right| \chi^n \rangle_R \tag{6.6}$$

where $f(R)$ is the electronic couplings from Eq. (6.5). The results are the elements in the Hamiltonian matrix. The number of times the integration in Eq. (6.6) had to be done was now reduced to

$$\frac{(N_{el}N_{vib})^2}{4} \tag{6.7}$$

typically almost a billion.

Integrating a product of B-spline expanded functions

Integrations of the kind[1]

$$\langle \psi_i \left| f(x) \right| \psi_j \rangle_x \tag{6.8}$$

are done a number of times, and it can be beneficial to see how they are actually calculated. ψ_i and ψ_j are expanded in B-splines, so the integral can be written as

$$\begin{aligned} &\int \sum_i c_i B_i(x) \cdot f(x) \cdot \sum_j d_j B_j(x) dx \\ &= \sum_i \sum_j c_i d_j \int B_i(x) \cdot f(x) \cdot B_j(x) dx \end{aligned} \tag{6.9}$$

In Eq. (6.9) all that is actually integrated is products of two B-spline functions multiplied with $f(x)$. The actual integration part of the problem does not explicitly involve the wavefunctions. Since Eq. (6.8) is typically calculated for a few thousand combinations of wavefunctions for each $f(x)$, the integrals in Eq. (6.9) are stored. If they are stored in a matrix, A, not only will it be banded, (see section 5.3), but it leads to rewriting Eq. (6.9) as a linear algebra problem

$$\vec{c}^T A \vec{d} \tag{6.10}$$

where $\vec{c}$ and $\vec{d}$ are the coefficients in the expansions, and A is a symmetric banded matrix with elements

$$A_{i,j} = \int B_i(x) f(x) B_j(x) dx$$

Using the case of the electronic dipole couplings, Eq. (6.5), as an example, $f(x) = x$, and A need only be calculated once.

6.2.3 The NBO couplings

The computations are not as straight forward for the non BO matrix elements.

$$\begin{aligned} H_{\eta,\xi} =& \frac{-1}{M} \left\langle \Psi^{\eta}_{tot} \left| \widehat{H}_{NBO} \right| \Psi^{\xi}_{tot} \right\rangle \\ =& \frac{-1}{M} \left(2 \left\langle \chi_m(R) \psi^i_e(x;R) \left| \frac{\partial \psi^j_e(x;R)}{\partial R} \frac{\partial \chi_n(R)}{\partial R} \right\rangle_{x,R} \right. \right. \\ &+ \left. \left\langle \chi_m(R) \psi^i_e(x;R) \left| \frac{\partial^2 \psi^j_e(x;R)}{\partial R^2} \chi_n(R) \right\rangle_{x,R} \right) \end{aligned} \tag{6.11}$$

[1] The variable x was used here, but this is a general example, and it is exactly the same for R.

The problem is the differentiation operators. The integrations in x,

$$f_1(R) = \left\langle \psi_e^i(x;R) \left| \frac{\partial \psi_e^j(x;R)}{\partial R} \right. \right\rangle_x \qquad \text{and} \qquad f_2(R) = \left\langle \psi_e^i(x;R) \left| \frac{\partial^2 \psi_e^j(x;R)}{\partial R^2} \right. \right\rangle_x \quad (6.12)$$

need the first and second derivated of the electronic wavefunction with respect to R. When the electronic wavefunction is expanded,

$$\psi_e(x;R) = \sum_i c_i(R) B_i(x) \quad (6.13)$$

the basis functions depend only on x, and the coefficients are functions of the internuclear distance, R. To differentiate $\psi_e(x;R)$ in R, the individual coefficients must be derivated. $c(R)$ is known on the integration grid, and a good way to interpolate and differentiate the function was to use a method from the python library[2]. The matrix, A from Eq. (6.10), containing the B-spline integrals, will simply be the overlap matrix, S from Eq. (5.5), which has already been calculated.

For the second term in Eq. 6.11 the integration over R will go exactly as in the dipole case. For the first term,

$$\left\langle \chi_m(R) \left| f_1(R) \left| \frac{\partial \chi_n(R)}{\partial R} \right. \right\rangle_R$$

the A matrix will be a bit different, with elements

$$A_{i,j} = \int B_i(R) f(R) \frac{\partial B_j(R)}{\partial R} dR$$

The derivatives of the B-splines were already calculated, for the BO Hamiltonian, so no further derivation is needed.

The Hermitian argument still stands, the final matrix is symmetrical and only the elements from the diagonal and up are needed. However, in the intermediate steps, there is no symmetry. This has no practical implication beyond making it harder to validate the results when writing the code. The electronic wavefunctions will still be even/odd after the derivation. Since the spatial symmetry/antisymmetry is for the x variable, the derivation in R will not change it. The difference from the dipole case is the lack of the x, which is antisymmetric. This means

$$\left\langle \psi_e^i \left| \frac{\partial^n}{\partial R^n} \right| \psi_e^j \right\rangle = 0, \quad \text{when} \quad i+j \quad \text{is an odd number.}$$

rather than for even numbers, as for the dipole couplings.

[2] scipy.interpolate.splev() and scipy.interpolate.splrep()

6.3 Truncation in space and energy

The size of the domain and the size of the basis sets depends on the problem. A wavepacket that is generated by the laser pulse must not be allowed to hit the edge of the box. The amount of time the system is propagated tells how far the wavepacket will get, and in that way decides the size of the box. The frequency and intensity of the laser determines how high energies the system can reach. Our eigenfunction basis needs to have functions of equally high energy to model the problem. To get eigenfunctions with higher energy, one needs to add more B-spline basis functions to the TISE basis set. This is the basic idea, but there is a few other considerations. There is a maximal separation between the B-spline knotpoints (see Section 5.3) if the eigenfunctions are to be smoothly drawn. For our H_2^+ model the required density is 10 $\frac{\text{knpts}}{\text{a.u.}}$ in the x domain, and 14 $\frac{\text{knpts}}{\text{a.u.}}$ in the R domain. Not all the BO eigenstates that are attained by diagonalisation can be included in the time propagation basis set. The states with lowest energy will be good eigenstates of the Hamiltonian. The highest states, however, are artifacts of the discretisation, and will vary markedly if the box size or the order is changed. We want to exclude these states from our eigenfunction basis. The question is how to recognise a bad eigenfunction. The density of states is given as $g(E_i) = \frac{2}{E_{i+1} - E_{i-1}}$. From theory [1, p 86] it is known that the density of states, for a free particle in one dimension, should go as

$$g(E) \propto E^{-\frac{1}{2}}, \tag{6.14}$$

E being the energy. For unbound states, the same behaviour is observed for the H_2^+ model, up to a certain point. For the highest energies the density of states will deviate from the expected behaviour, at which point we leave the states out of the basis set. Figure 6.2 shows an example of how the density of state can look. For the dissosiating states, one sees an $E^{-\frac{1}{2}}$ tendency. However, at $E \sim 0.5$ a.u., one observes irregular behaviour, which we interpret as the eigenfunctions going bad.

When building the basis sets, one makes them as small as possible, without violating the demands outlined in this section. Table 6.3 lists the domain and basis specifications for the simulations we ran in this thesis.

Table 6.1: The size of the domains in electronic coordinates, x, and nuclear coordinates, R. The number of seventh order B-spline functions in the TISE basis sets, and the number of BO eigenstates in the TDSE basis set is also included.

	min	max	Number of B-spline	Number of el/vib eigen-
	(a.u.)	(a.u.)	functions	functions
x	-120	120	480	200
R	0.5	25	350	300

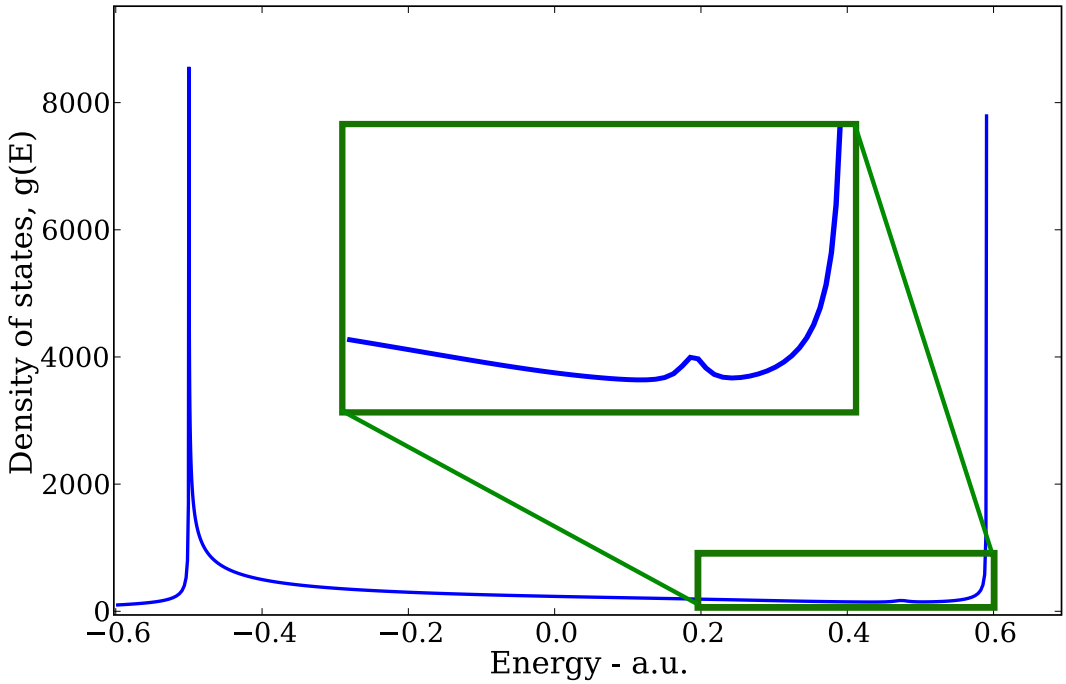

Figure 6.2: The density of vibrational states for the $1g$ potential curve. As may be seen from the figure, the bound states, (energies below 0.5 a.u.), will not have the $\frac{1}{\sqrt{E}}$ tendency. For $E \sim 0.5$ a.u., there are clear signs of unphysical behaviour, and at $E \sim 0.6$ a.u. $g(E)$ explodes. That high energies were not needed for the $1g$ in our problems, since the population on those states were negligible. The final cut was made at $E \sim 0.3$ a.u., corresponding to a basis set of 300 BO eigenfunctions.

Chapter 7

Resonance Enhanced Multi-Photon Ionisation (REMPI) in H_2^+

In 2005, Palacios *et al.* published an article called *Two-photon ionization of* H_2^+ *by short laser pulses* [15](see also [32, 31]). We attemted to reproduce some of the interesting results reported, using our 1D model.

7.1 Article summary

Doing 3D calculations in the BO approximation, Palacios *et al.* simulated an H_2^+ molecule ionised from the vibrational ground state by two photons. They did this for a wide range of laser frequencies, $\omega = 0.45 - 1.0$ a.u., several different intensities, $I = 10^{10} - 10^{14}$ Wcm^{-2}, and pulse durations, $T = 0.5 - 10$ femtoseconds (fs). Two different methods were used, lowest order perturbation theory, (LOPT), and solving the time dependent Schrödinger equation, (TDSE). Both these methods were used to find the differential cross section as a function of the kinetic energy release (KER) of the protons, i.e. the kinetic energy of the protons when they are far apart. The results were compared.

Some of the more interesting results were found for frequencies near $\omega = 0.8$ a.u., and these are the results we intend to reproduce with our 1D model. Figure 7.1 schematically shows the BO picture of the scenario.

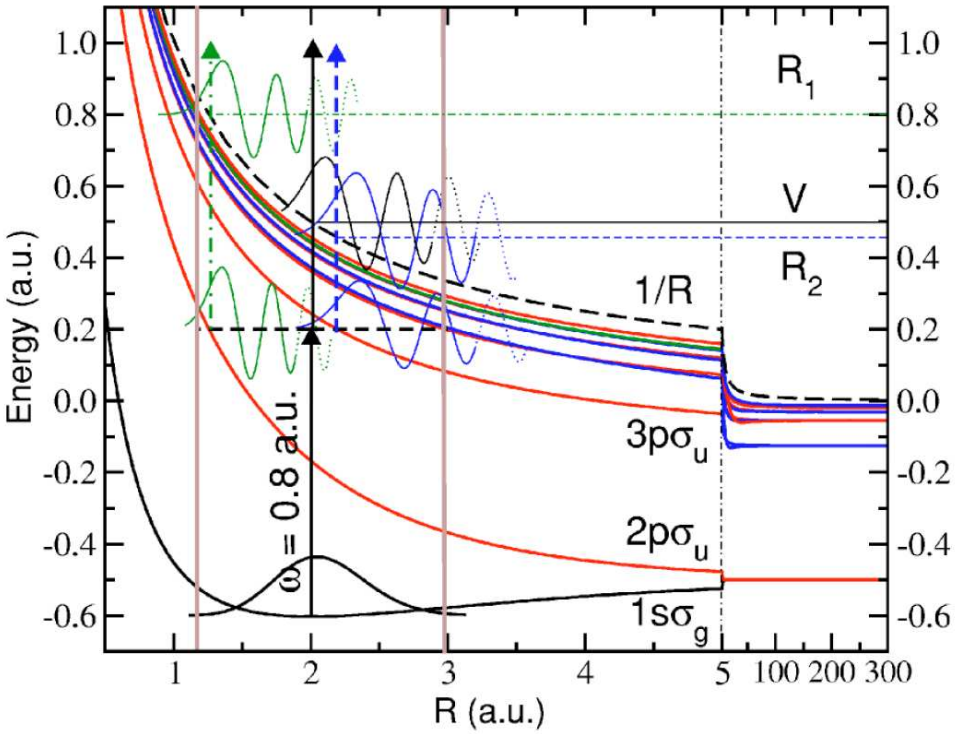

Figure 7.1: Electronic energy curves in H_2^+. The arrows symbolise the photons that ionise the system. The dashed curve, $\frac{1}{R}$, is the ionisation threshold. The shape of the initial wavefunction is plotted, to show for what internuclear distances transitions are likely to occur [15].

As can be seen in Fig. 7.1, if the system absorbs two photons, the electronic energy will be over the ionisation threshold, $\frac{1}{R}$, (the dashed curve in the figure), causing a Coulomb explosion of the molecule. Palacios *et al.* calculated the energy spectra of the protons after the ionisation. The energy spectra arrived at in [15] showed some obvious peaks, see Fig. 7.2. Information may be gleaned from these, since the peaks in the energy spectrum may be mapped back to where on the R domain the ionisation occured. This can be done by using the classical relation

$$E \sim \frac{1}{R} \tag{7.1}$$

to estimate the final energies of the protons. The approximation stems from the fact that if the electron is removed, the potential energy will simply be $\frac{1}{R}$. In the limit when $R \to \infty$, all the potential energy of the nuclei will have become kinetic energy. Since it relies on the assumtion that the nuclei have no kinetic energy initially, and that they are not notably disturbed by the stripping of the electron, this will not be exact. The peaks at energy $E \sim 0.5$ a.u., which are called V in Figure 7.2, are mapped back to $R \sim 2$ a.u. That

corresponds to where there is a maximum in the population of the wavefunction on the $1s\sigma_g$ energy surface. It is obvious that it will be a higher ionisation probability if there is more population to ionise. One may expect the spectrum to be a picture of the initial population, but that does not explain the peaks that are denoted R_1 and R_2.

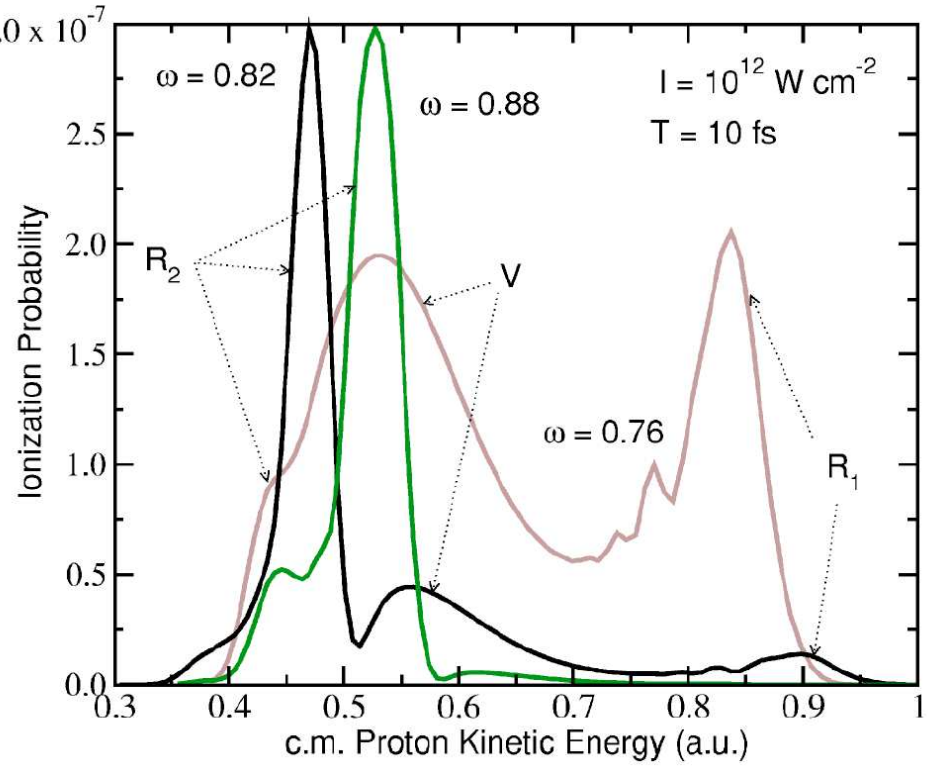

Figure 7.2: KER spectra of the protons after the two-photon ionisation. The peaks in the spectra, marked R_1 and R_2, may be mapped back to resonant transitions, see Fig. 7.3 [15].

The kind of ionisation we are looking at is often called REMPI, or resonance enhanced multi-photon ionisation. Palacios *et al.* explains that the additional peaks stem from enhanced transitions caused by resonances in the system. The peaks are named R_1 and R_2 because they can be mapped back to internuclear distances, $R_1 \sim 1$ a.u. and $R_2 \sim 3$ a.u., respectively (see Figure 7.3). For these R-values there will be a resonant transition, since the distance in energy between the ground state and the $2p\sigma_u/3p\sigma_u$ electronic energy curves, respectively, matches the photon energy, $\omega \sim 0.8$ a.u.

The enhanced transition at the resonances follows from the fact that a one-photon transition is more likely than a two-photon transition. In fact, *two* one-photon transitions are still a lot more likely than a direct two-photon transition. The electron is removed in two steps. A photon is absorbed to bring the electron to the intermediate state, before the

molecule is fully ionised by another photon[1]. The only reason why the resonances do not dwarf the two-photon channel, is that in the ground state, around $R \sim 1$ a.u. and $R \sim 3$ a.u., where the resonant transitions occur, there is very little population, see Fig. 7.3.

7.2 The scenario in 1D

We wanted to see if our model could reproduce the REMPI characteristics described in Palacios' article, [15]. The scenario is relatively simple, and the mechanisms behind the results are understood. That makes the problem ideal for testing our model.

Due to the fitting of the $1g$ and $2u$, similar resonances to those reported by Palacios *et al.* are present in the one dimensional model. We were able to use almost the same laser settings, although the pulse duration had to be reduced slightly. The computer resources at hand made it impractical to use too big a domain in the x variable, so the pulse duration was set to 7 fs instead of 10 fs. This may cause the resonances to be somewhat broader, and may also reduce the total ionisation yield. The specifications for the laser pulse were otherwise taken from the article,

$$\begin{aligned} \text{Laser frequency:} \quad & \omega = 0.76 \quad 0.82 \quad \text{and} \quad 0.88 \text{ a.u.} \\ \text{Intensity:} \quad & I = 10^{12} \text{ Wcm}^{-2} \\ \text{Pulse duration:} \quad & T = 7 \text{ fs} \end{aligned}$$

The energy spectra of the nuclei may be found from the vector of expansion coefficients describing the wavefunction after the pulse. In the BO approximation there is a nuclear energy spectrum for each electronic state. It is calculated by the simple formula,

$$\frac{dP}{dE}(E_m) = \frac{2|c_m|^2}{E_{m+1} - E_{m-1}} \tag{7.2}$$

where $|c_m|^2$ is the expansion coeffisient squared, Eq. (6.3), or in other words, the probability of being in the vibrational state m. E_m is the corresponding nuclear energy, i.e. $E_{tot} - E_e(R \to \infty)$ for state m. In the formula the probability is multiplied with the density of states, $g(E_m) = \frac{2}{E_{m+1} - E_{m-1}}$. It is then interpolated to find a continuous distribution. This is done for all the electronic states in the continuum, and added up. The same can be done for dissociative states below the continuum. The electronic spectrum may be found in a similar way.

[1] The direct two-photon peaks are denoted V, because the intermediate state is a "virtual" state [15].

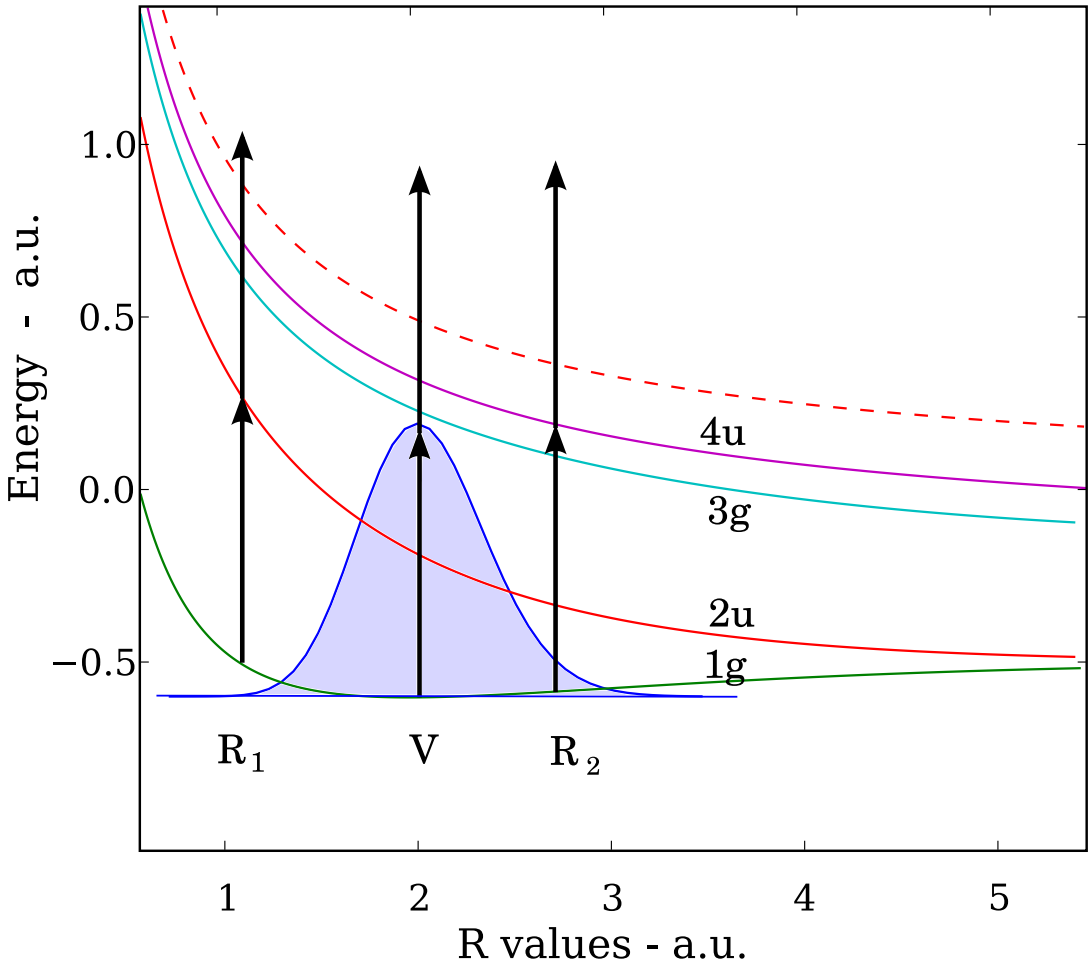

Figure 7.3: An H_2^+ molecule in the ground state, ionised by an $\omega \sim 0.8$ a.u. laser pulse. The four lowest electronic energy curves are drawn, as well as the ionisation limit (dashed) and the ground state wavefunction (not to scale). The arrows illustrate photon absorptions. There is a transition resonance between the ground state and $2u$ at $R_1 \sim 1.1$ a.u., and one between the ground state and $4u$ at $R_2 \sim 2.8$ a.u. The direct two-photon ionisation will be possible wherever there is population in the ground state, but the arrows are placed at $V = 2.1$ a.u. since the population, and ergo the transition probability is highest there.

7.3 Results

The TDSE was solved for each of the three laser frequencies, and the nuclear energy spectrum in the continuum was calculated, see Fig. 7.4. The expexted results was to find

three peaks, corresponding to the resonances at R_1 and R_2, and the direct two-photon transition at V. The position of the resonance peaks in the spectra was expected to move when the frequency was changed, since the resonant transitions will occur at smaller R when the frequency is increased. For $\omega = 0.76$ a.u., the matching energy gap between the $1g$ and the $2u$ is at $R_1 = 1.16$ a.u., whereas for $\omega = 0.88$ a.u., the resonant transition will take place at $R_1 = 0.94$ a.u. The position of the two-photon peak, (V), was expected to remain the same, since the transition does not depend on any intermediate states. The height of the peaks were also expected to change with the frequency, as the height depends on the population that may be transferred from the $1g$ at the given internuclear distance. The population on the $1g$ is largest at $V = 2.1$ a.u., so one expects the R_1 and R_3 peaks to be higher the closer the resonances are to this internuclear distance.

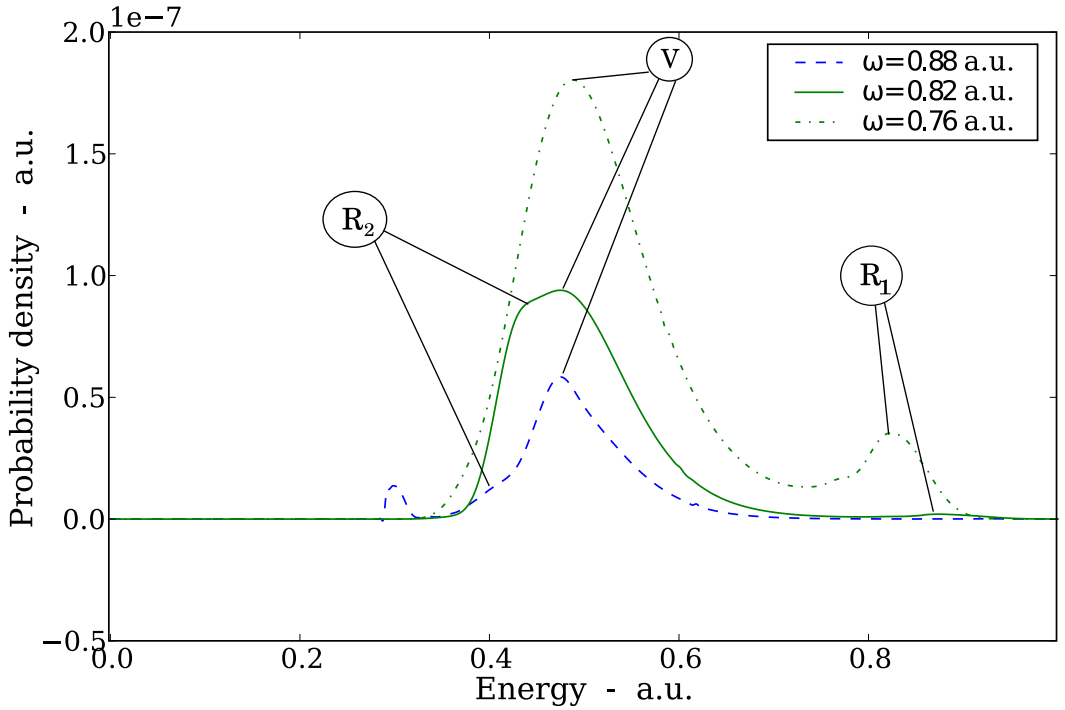

Figure 7.4: Nuclear KER spectra for H_2^+ ionised by a laser pulse of frequency $\omega = 0.76, 0.82$ or 0.88 a.u. The REMPI peaks are marked with R_1 and R_2, while V shows the direct two-photon ionisation peaks. For comparison with the 3D simulation, see Fig. 7.2.

Much of this was apparent in the result. The position of the direct two-photon peak, denoted V in Fig. 7.4, does not change with the frequency, but stays at $E \sim 0.5$ a.u., exactly as expected. Its height also matches well with what was reported in [15]. The $1g - 2u$ res-

onance peak, denoted R_1, is clear at $E \sim 0.82$ a.u. for $\omega = 0.76$ a.u. For $\omega = 0.82$ a.u. it is much smaller, and positioned at $E \sim 0.9$ a.u., while for $\omega = 0.88$ a.u. it is too small to see. This is directly in accordance with expectations and Palacios' article, though the height of the peaks is noticably lower in our case. The resonance from R_2, which overlaps with the direct two-photon transition, is noticable only as a knee on the V peak, and only for the two highest frequencies. Compared to the results from the article, the peaks are again very low, and since they almost overlap with the V transition, the peaks are hard to distinguish. The $4u$ is not fitted to the corresponding 3D energy curve, and one must assume it does not ideally mimic the $3p\sigma_u$ potential curve in the 3D model. This may account for some of the discrepancies between the 3D results and ours. It is harder to tell why both the resonance peaks are so much lower than reported in [15]. However, one cannot expect a 1D model to give quantitatively the same results as the full 3D model, and we are satisfied with such a good qualitative agreement. There is a small peak at $E \sim 0.3$ a.u. It is not mentioned in [15], and it is caused by a one-photon ionisation channel that opens for large values of R.

To see the resonances more clearly, we calculated the dissosiation spectra. This will boost the transitions that have an intermediate resonant state, i.e. R_1 and R_2, and remove the direct two-photon transition, V. As we can see from Figure 7.5, the resonances stand out very clearly. The resonance peaks move towards higher energies when the frequency is increased, and this time the R_2 peaks are visible for all three frequencies. The approximative mapping between energy and internuclear distance, $E \sim \frac{1}{R}$ will of course no longer be valid, since the electron is still present in the system. As a result, the structures in the spectra are shifted sightly toward lower energies, compared to the ionisation spectra. In the $\omega = 0.88$ a.u. spectrum, there is an additional peak at $E \sim 0.35$ a.u. It is caused by a resonant transition to the $6u$ curve.

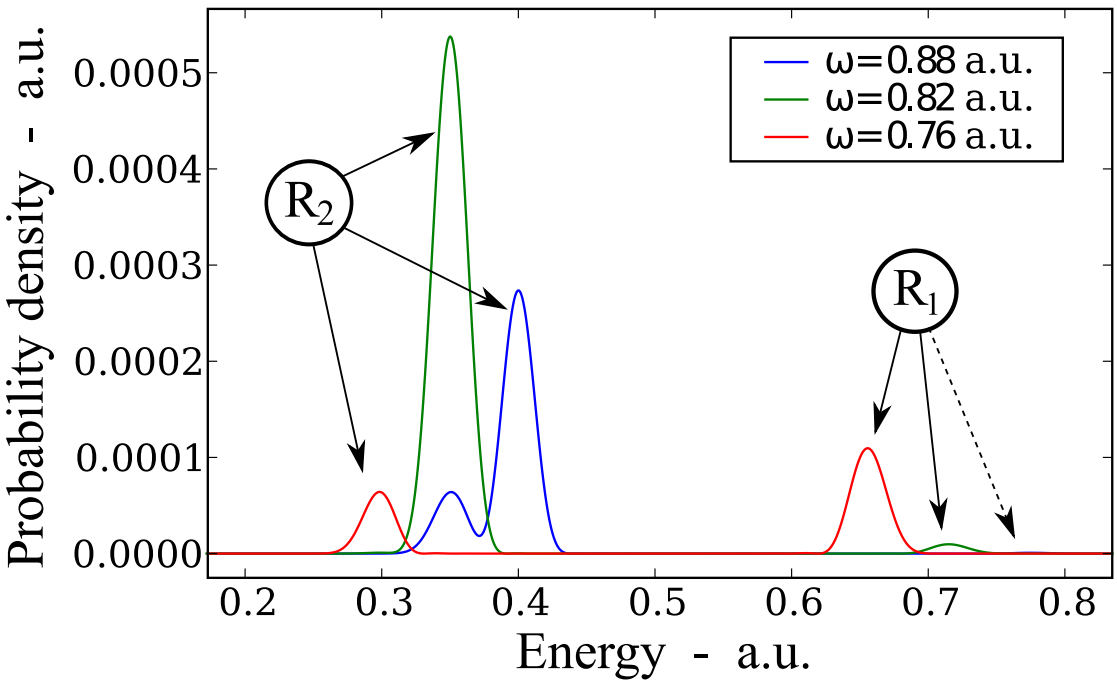

Figure 7.5: The dissosiation spectrum for H_2^+ after a 7 fs laser pulse of frequency $\omega = 0.76$, 0.82 or 0.88 a.u. The peaks marked with R_1 are caused by transitions between the $1g$ and the $2u$ potential curves. The dotted arrow points to a peak on the 0.88 a.u. spectrum that is visible when magnified. The peaks denoted R_2 corresponds to transitions between $1g$ and $4u$.

Chapter 8

Wave Packet Interference (WPI) in H_2^+

In a recently published article by Førre *et al.*, *Nuclear Interference in the Coulomb Explosion of H_2^+ in Short vuv Laser Fields* [16], modulations in the ionisation spectrum of H_2^+ are reported. The modulations are caused by interference between two nuclear wavepackets on the $3d\sigma_g$ energy surface. The interference occurs because there are two open paths to the $3d\sigma_g$ dissosiation channel, (see Fig. 8.1). This leads to two overlapping wavepackets of the same energy, that are out of phase with each other. The constructive and destructive interferences between them result in modulations in the dissosiation/ionisation energy spectra of the protons.

8.1 Article summary

The article describes H_2^+ in the BO approximation, interacting with a laser pulse of duration 10 fs - 16 fs, and a central frequency of $\omega = 0.32$ a.u. The electronic motion is modelled in three dimensions, while for the nuclei, only vibrational motion is included. The nuclei are aligned with the polarisation axis of the laser field, and not allowed to rotate. This approximation is justified, as the rotational motion is negligible for the pulse durations used in the simulation. The initial state of the system is the Franck-Condon wavepacket, χ_{FC}, described in see Eq. (3.8). The wavepacket will propagate to the right with time, (see Fig. 3.6). For the given laser frequency and duration, certain transitions, illustrated on Figure 8.1, will dominate in the dynamics of the system.

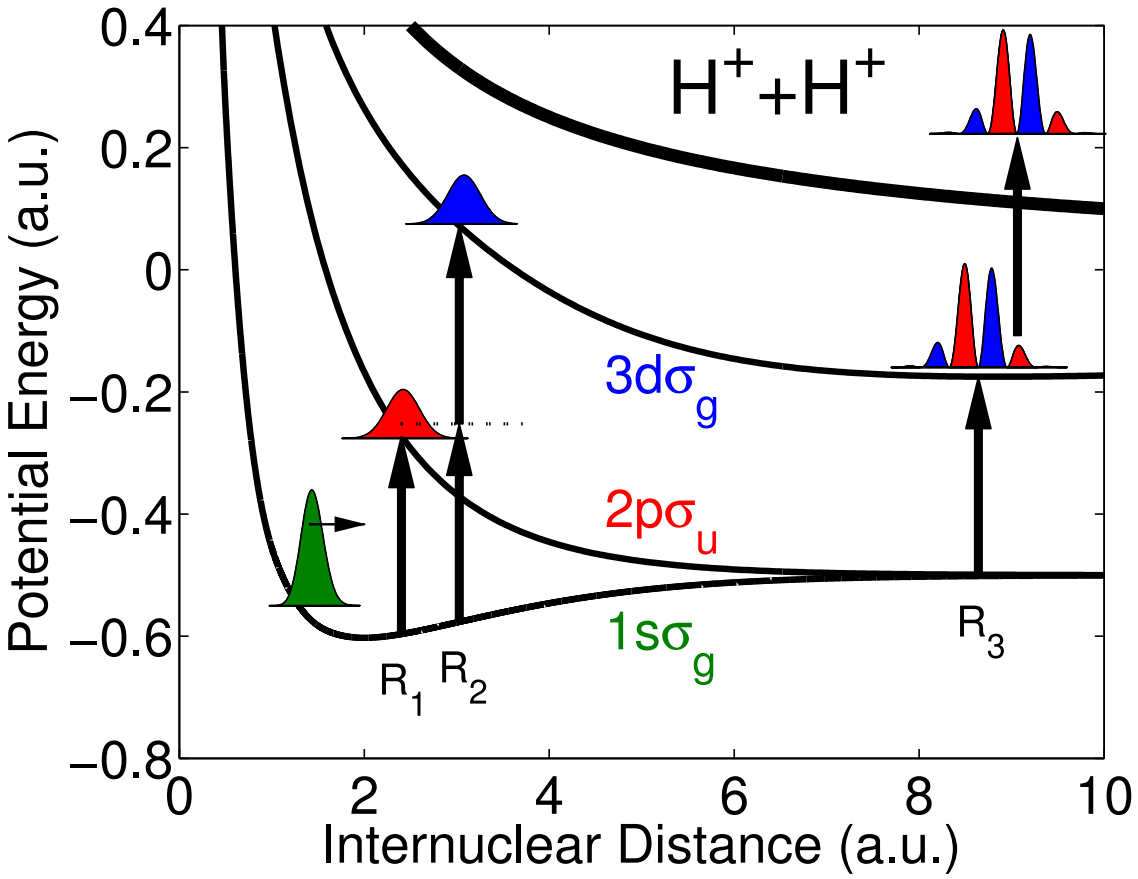

Figure 8.1: Schematic figure of the dominating transitions in H_2^+ for a laser pulse with frequency $\omega = 0.32$ a.u. Two different ionisation channels pass through the $3d\sigma_g$ state, and create interference. All population is initially in the ground state. The laser will bring a wavepacket from the electronic energy curve $1s\sigma_g$ to the $2p\sigma_u$ curve at internuclear distance R_1 through a resonant one-photon transition. A resonant two-photon transition at R_2 brings a wavepacket from $1s\sigma_g$ to $3d\sigma_g$. This wavepacket will interfere with a wavepacket that is tranferred from $2p\sigma_u$ at R_3.

At $R_2 \sim 3.1$ a.u. there is a resonance for a two photon absorption, bringing a wavepacket from $1s\sigma_g$ directly to the $3d\sigma_g$ curve. There is an alternative path to the $3d\sigma_g$ potential curve, namely by two separate one photon absorptions, one at $R_1 \sim 2.4$ a.u., lifting the wave packet onto $2p\sigma_u$, from where it moves to larger R, and another resonance with the $3d\sigma_g$ curve at $R_3 \sim 8.6$ a.u. The laser frequency was chosen because it fits the energy gap between $2p\sigma_u$ and $3d\sigma_g$ at R_3, opening this second transition path. For pulse durations longer than 10 fs, but less than 16 fs, the contributions from each path are approximately the same. The wavepackets interfere, creating a modulated wavepacket, which in turn leads to the characteristic modulations in the $3d\sigma_g$ dissosiation energy spectra, Fig. 8.2. A third

photon may ionise the system, and an image of the modulated wavepacket is reflected in the CE channel ($H_2^+ \rightarrow H^+ + H^+ + e^-$) as well, see Fig. 8.3.

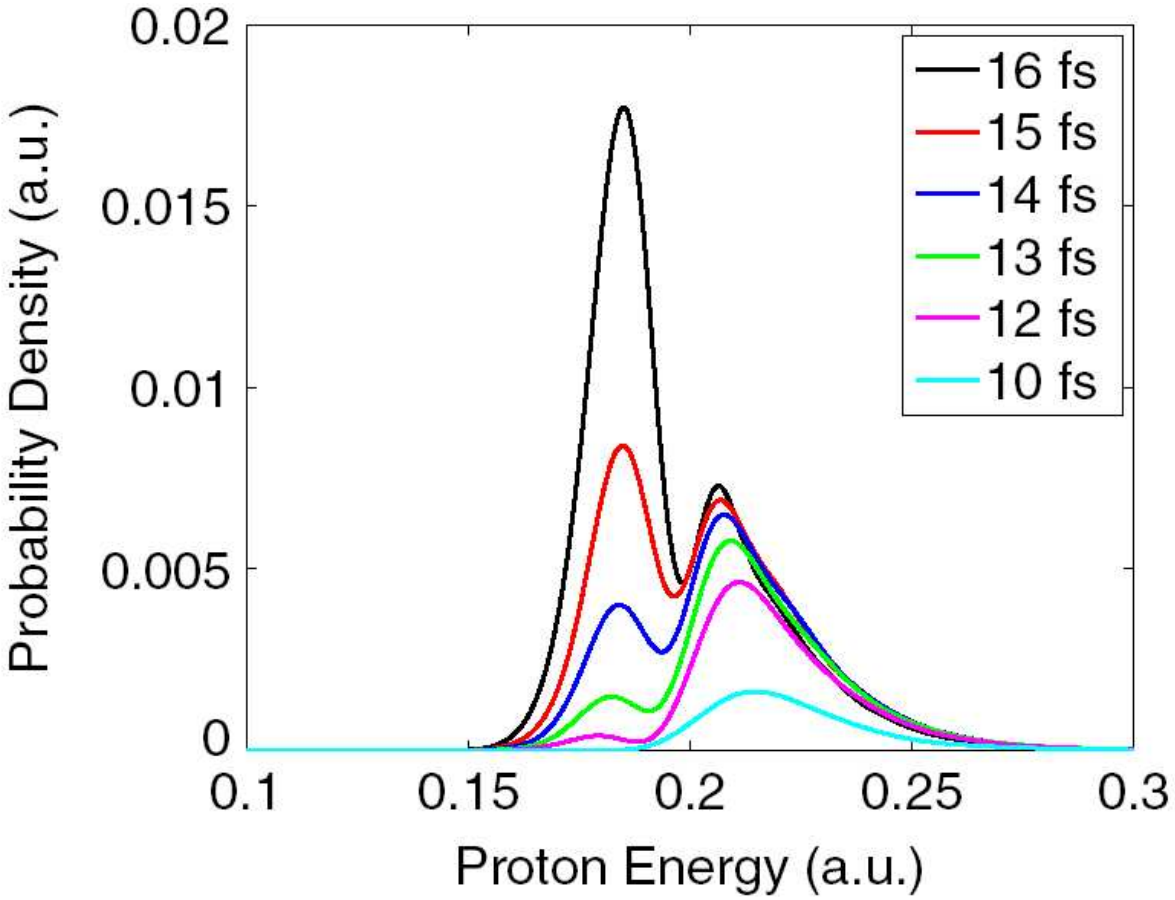

Figure 8.2: KER spectrum of the $3d\sigma_g$ dissosiasion channel, for an H_2^+ molecule in a laser field with central frequency $\omega = 0.32$ a.u., intensity $I = 1 \cdot 10^{12}$ Wcm^{-2} and pulse durations from 10 to 16 femtoseconds.

The dissosiation spectra in Fig. 8.2 show two peaks at proton energies 0.18 a.u. and 0.21 a.u. For a pulse duration of 10 fs, there is only one peak. This is because the wavepacket on $2p\sigma_u$ did not have time to propagate to R_3, thereby effectively closing that transition path. With only one wavepacket on the $3d\sigma_g$ electronic energy curve, there could be no wave packet interference (WPI), i.e. no modulations are visible in the energy spectrum.

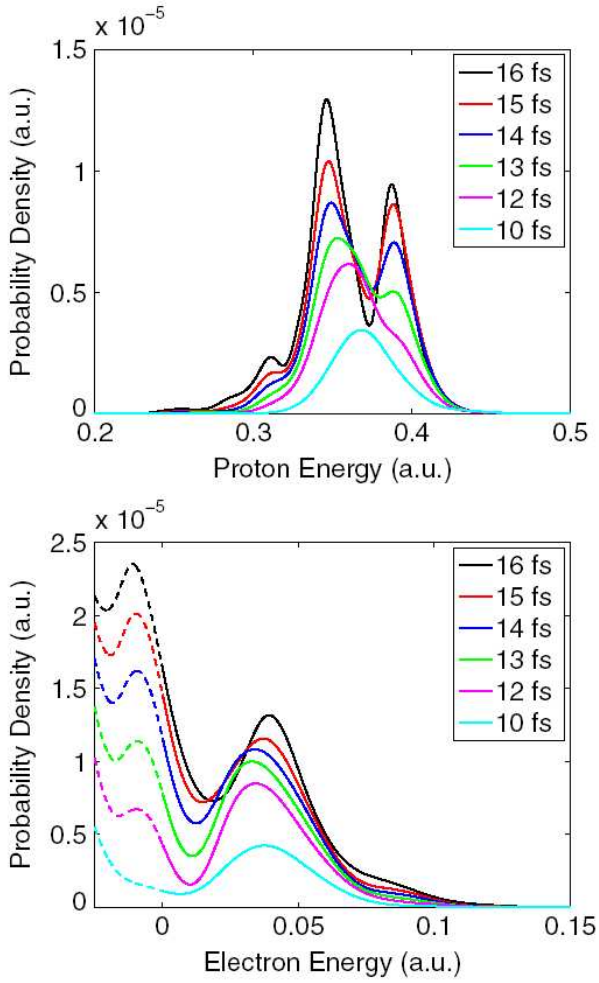

Figure 8.3: KER spectrum after ionisation of H_2^+ by an $\omega = 0.32$ a.u., I = $1.0{\cdot}10^{12}$ Wcm^{-2} laser pulse, for different pulse durations. Upper panel: The proton energy spectra are clearly modulated for the pulse durations longer than 10 fs. Lower panel: Similar modulations are discernible in the electron spectra, as demanded by the conservation of energy principle.

The modulations seen in the dissosiation spectra in Fig. 8.2 are also obvious in the ionisation spectra drawn in Figure 8.3. This is because the system may be ionised from the $3d\sigma_g$ curve, and a signature of the wavepackets are transferred to the continuum. The modulations are also visible in the electron spectra. As a direct consequence of the conservation of energy principle, the structures in the proton energy spectrum also appear in the electronic energy spectrum.

8.2 The scenario in 1D

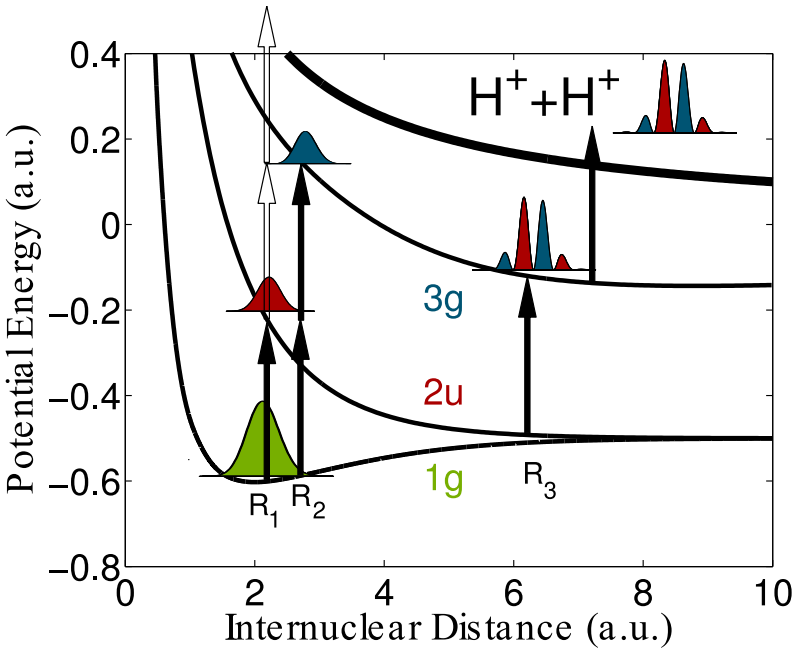

Figure 8.4: Scematic figure of the dominating transitions in H_2^+ for a laser pulse with frequency $\omega = 0.355$ a.u. Two different ionisation channels pass through the $3d\sigma_g$ state, and create interference. There is an enhanced three-photon ionisation channel at R_1 (white arrows).

We have studied a similar scenario in 1D. However, instead of starting with a Franck-Condon wavepacket, as in [16], we used the H_2^+ vibrational ground state as our initial state. Other adjustments had to be made as well, and chief among them was changing the laser frequency. The frequency was chosen so that the photon energy would match the energy gap between $2p\sigma_u$ and $3d\sigma_g$ for large R. The corresponding energy gap in the 1D model, i.e. between $2u$ and $3g$, is larger than in 3D. To make the R_3-transition available, the laser frequency had to be increased to $\omega = 0.355$ a.u. This in turn led to changing the other laser specifications, in order to achieve WPI on the $3g$ electronic energy curve. The laser pulse settings we ended up with were

$$\begin{aligned} \text{Laser frequency:} \quad & \omega = 0.355 \text{ a.u.} \\ \text{Intensity:} \quad & I = 3.5 \cdot 10^{12} \text{ Wcm}^{-2} \\ \text{Pulse duration:} \quad & T = 10 \text{ fs} \end{aligned}$$

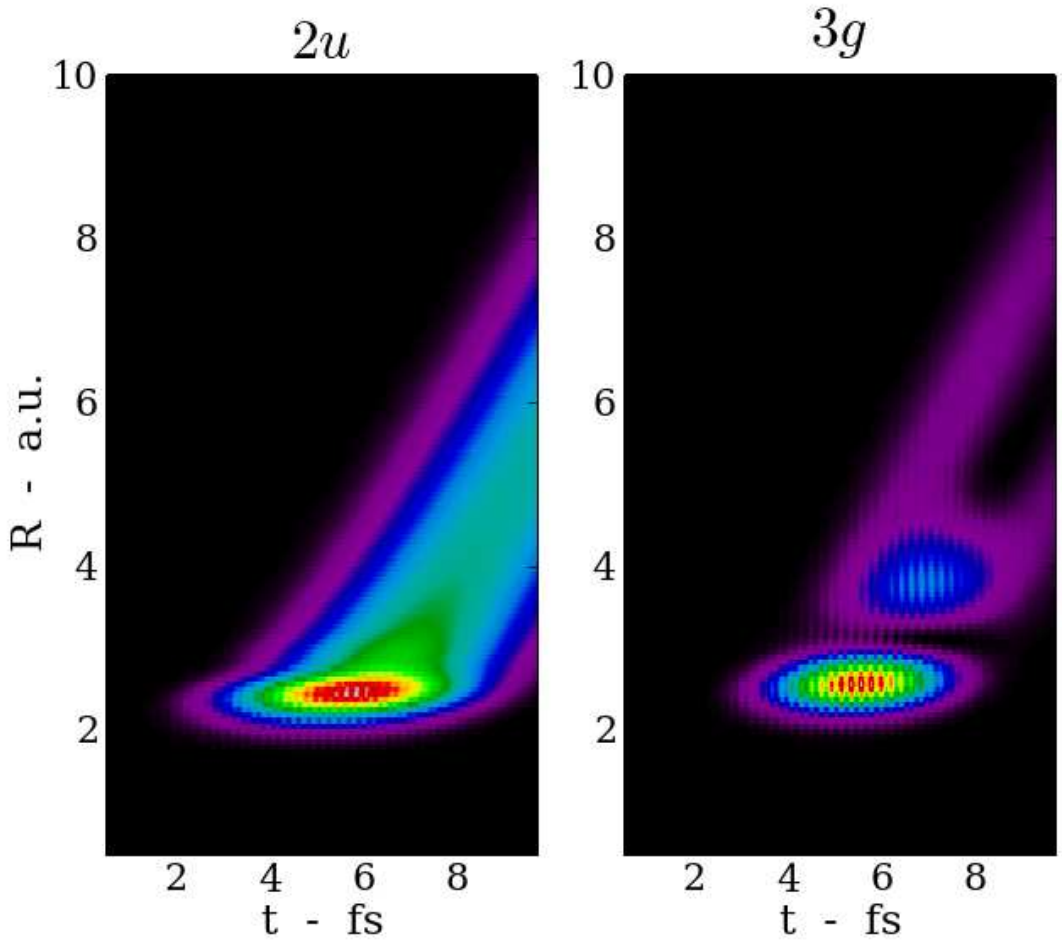

Figure 8.5: A qualitative plot of the probability density as a function of time (x-axis) and internuclear distance (y-axis). On the left, the population on the $2u$ BO curve, on the right, the population on $3g$. (Though it is not apparent on the figure, the population is 3-4 orders of magnitude larger on $2u$ than on $3g$.) The population around $R \sim 2.5$ a.u., which corresponds to the one- and two-photon resonances, (left and right, respectively), seems to be strongly dependent on the intensity of the electric field. Both the overall carrier-envelope, $\sin^4(\frac{\pi t}{T})$, and the oscillations of the field, $\cos^2(\omega t)$, can be seen in the probability density. Population propagating toward larger internuclear distances are clear on both plots. However, while the left plot shows a smooth wavepacket, the wavepacket on the right have a more complex structure, caused by the interference from a second wavepacket.

8.3 Results

When looking at how the probability density changes with time and internuclear distance, Fig. 8.5, the resonances with one and two photons show up clearly. The left plot shows the population on $2u$, and the right plot shows the population on $3g$. The intense bands at $R \sim 2 - 3$ a.u. are caused by the resonant transitions at R_1 (left plot) and R_2 (right plot), (see Fig. 8.4). It is interesting to see how the population in these bands mimic the behaviour of the laser pulse. The population is strongest in the middle of the pulse, and disappears at the beginning and the end. This is the exact behaviour of the intensity profile of the laser pulse, which goes as $\sin^4(\frac{\pi t}{T})$. Upon closer examination, it is also possible to see more rapid oscillations modulating the bright band in the figure. What we see corresponds to the actual oscillations of the electric field, $\cos(\omega t)$, or rather the oscillations of the intensity, which goes as the square of the field strength. The one photon resonance between the ground state and $2u$ gives a much stronger contribution than the two photon resonance between the ground state and $3g$. The population is almost 10^4 times larger in the first excited electronic state than in the second. In both of them, however, the population can be seen propagating toward larger R values. Notice, however, that the shape of the wavepacket on $3g$ is distorted toward the end of the pulse. This occurs because the wavepacket interferes with another wavepacket that is transferred from $2u$ at R_3. The shape of the resulting wavepacket after the laser pulse is depicted in Fig. 8.6.

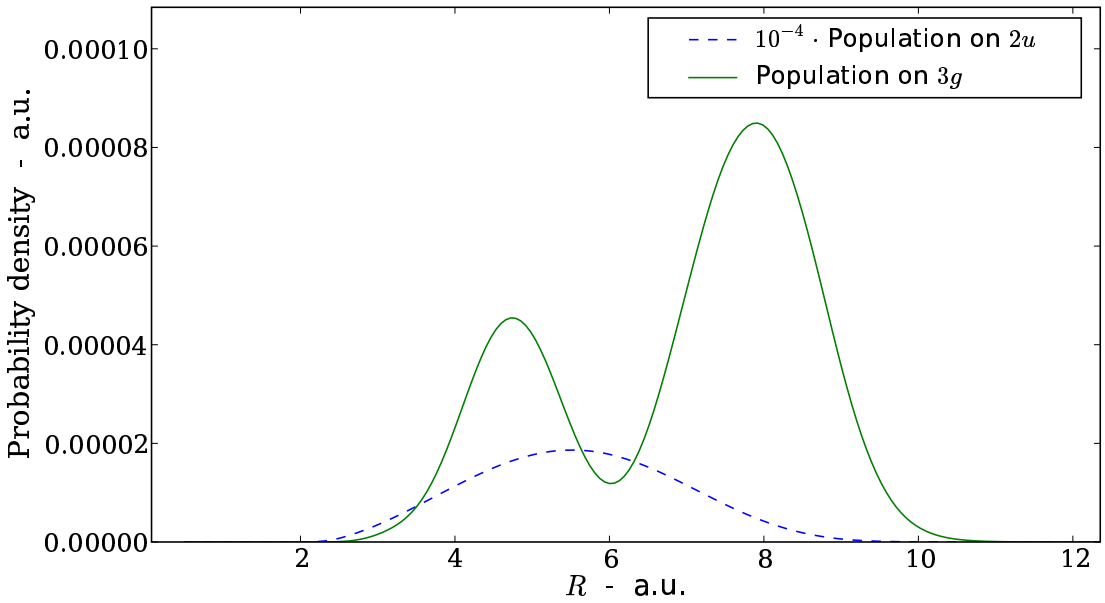

Figure 8.6: The probability density on the $3g$ (solid) and $2u$ (dashed) states, after the laser pulse. Whereas the population on $2u$ form a typical wavepacket moving to the right, the wavepacket on $3g$ is modulated. The modulation, as described in the text, is caused by WPI.

The spectrum attained for the $3g$ curve, Figure 8.7, shows exactly the same characteristics as were reported in [16]. The energies in Førre's article are centered around $E = 0.2$ a.u., cf. Fig. 8.2, while our energies are centered around $E = 0.25$ a.u. The reason for the discrepancy is the laser frequency, which is higher in our case. The asymptotical electron energy is approximately the same in both cases, so the the extra photon energy goes to the nuclei.

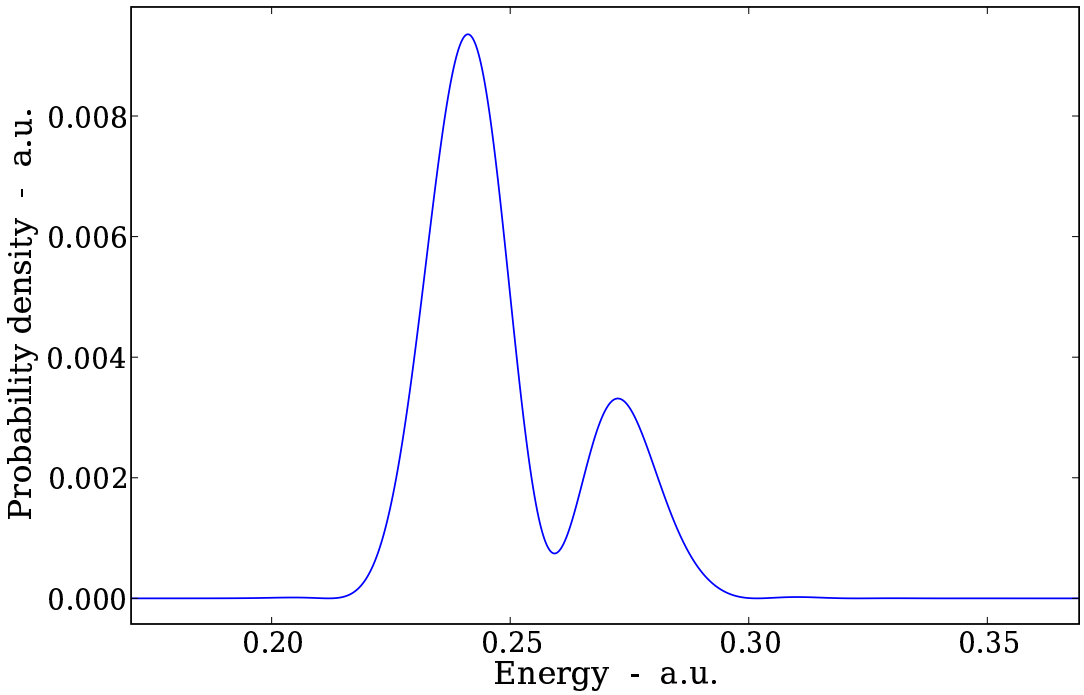

Figure 8.7: The proton energy distribution on the $3u$ after dissociation. The two peak structure is the same as in [16], see Fig. 8.2.

The peaks are visible in the Coulomb explosion spectrum as well, both for the electron (Fig. 8.9) and the nuclei, but as can be seen in the proton spectrum in Figure 8.8, the right peak is dominant. This is caused by ionisation through a rivaling channel (the white arrows in Fig. 8.4), in all likelihood the two-photon ionisation directly from the $2u$ electronic curve[1]. It should occur at $R \sim 2.2$ a.u., which corresponds to a proton energy $E \sim \frac{1}{R} \sim 0.46$ a.u., which is in agreement with the results. In [16] this channel is not contributing to the spectrum, since a lower frequency was used, and the transition did not reach the continuum. We made an attempt to disentangle the two ionisation channels. The energy spectrum is a sum of the spectra for each electron curve in the continuum. If the different ionisation channels have different electron energy, it is possible in a BO model to separate the channels, and to look at their contributions isolated. In this case, the direct three-photon ionisation at $R \sim 2.2$ a.u. leads to a low electron energy, whereas the transitions from $3g$ leads to a higher electron energy. As a consequence, we were able to

[1] This transition is the three-photon equivalent of the two-photon resonances described in the previous chapter.

plot the kinetic energy spectrum without the contamination from the direct three-photon transition, in Figure 8.10.

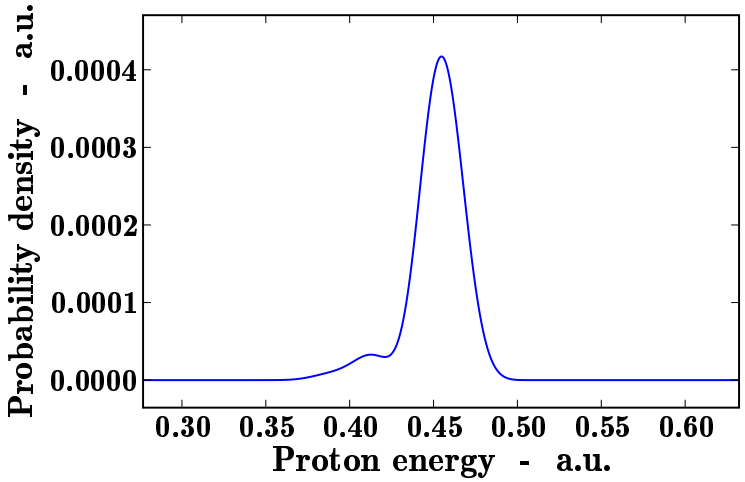

Figure 8.8: The proton energy distribution after a Coulomb explosion of H_2^+, for a laser pulse of frequency $\omega = 0.355$ a.u., a field amplitude of $E_0 = 0.01$ a.u. and a pulse duration of 10 fs. The two peaks are caused by one photon ionisation of two wave packets in $3g$, though the right peak is amplified by the two photon ionisation of a wavepacket on $2u$.

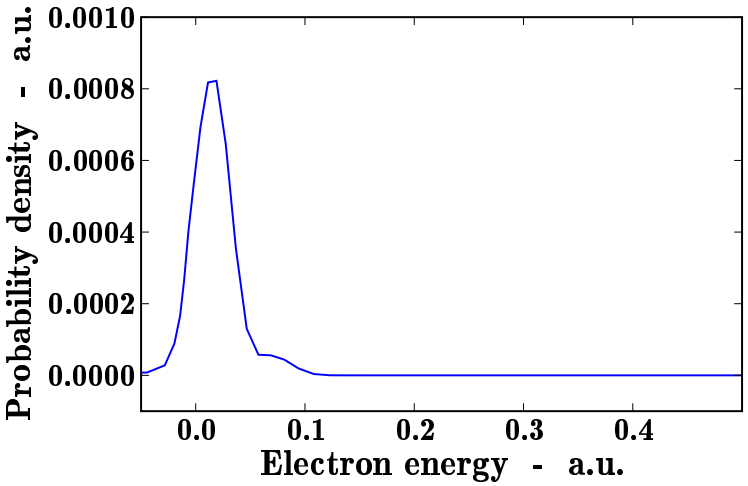

Figure 8.9: The electron energy distribution after ionisation of H_2^+.

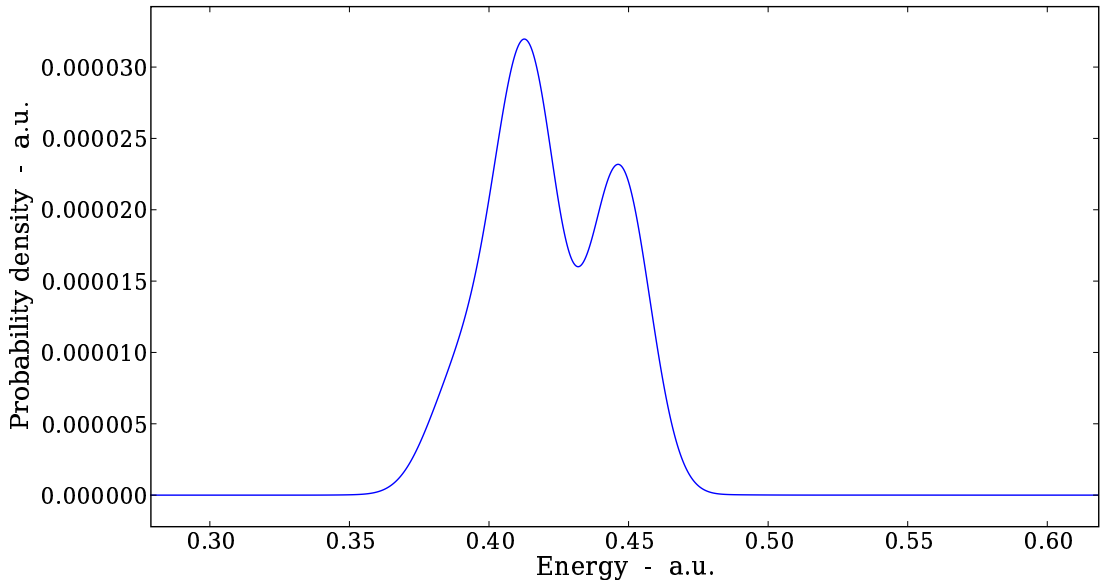

Figure 8.10: The proton energy distribution after a Coulomb explosion of H_2^+, showing only the contribution from the $3g$ channel. It would not be possible to make such a distinction in an experiment, but since the two ionisation channels results in somewhat different energies of the electron in the continuum, it is possible to disentangle the two processes in the calculated results.

Our model successfully reproduces the WPI phenomenon discovered in the 3D simulations that Førre *et al.* reported in [16]. This would have been difficult if the model had used constant softening parametres, as the lowest electronic energy curves, where most of the dynamics occured, would have been very different from the curves in the 3D model, see Fig 4.3.

8.4 Non-Born-Oppenheimer effects

We wanted to decide if the Born-Oppenheimer approximation was valid for this scenario. One of the foundations of the approximation is that the nuclear motion is much slower than the electronic motion. The classical speed of the particles can be estimatied from the kinetic energy. The peaks in the continuum spectra for protons (Fig. 8.8), and electrons (Fig. 8.9), suggest the kinetic energies

$$E_p^{kin} \sim 0.45 \text{ a.u.}$$
$$E_e^{kin} \sim 0.015 \text{ a.u.}$$

Classically this corresponds to the speeds

$$v_p = \sqrt{\frac{2E_p^{kin}}{\mu}} \sim 0.03 \text{ a.u.}$$
$$v_e = \sqrt{2E_e^{kin}} \sim 0.17 \text{ a.u.}$$

The validity of the BO approximation when $v_e \sim 6v_p$ is questionable.

From the dissosiation spectrum on the electronic energy curve $3g$, cf. Fig. 8.7, one can find the most likely total energy (E_{tot}) of the dissosiated system. $E_{tot} = E_e + E_p$, where the electronic energy is $E_e(R \to \infty) \sim -0.125$ a.u. after the dissosiation, and the proton energy, from the spectrum is $E_p \sim 0.25$ a.u. This gives us a total energy of $E_{tot} \sim 0.125$ a.u. This is above the threshold for ionisation. If the electrons and protons could exchange energy after the pulse due to the non-BO coupling, a Coulomb explosion could occur. The high proton energy may suggest that the nuclei are dissosiating so fast that the electronic wavefunction does not have time to adjust adiabatically to the changes, as the BO approximation assumes it does.

We wanted to test whether the approximation is justified or not. The WPI scenario was run again with non-BO couplings included. The spectrum (Fig. 8.11) is subtly different from the BO spectrum, however, it is not constant with time, i.e. it changes if the system is propagated further in time after the pulse.

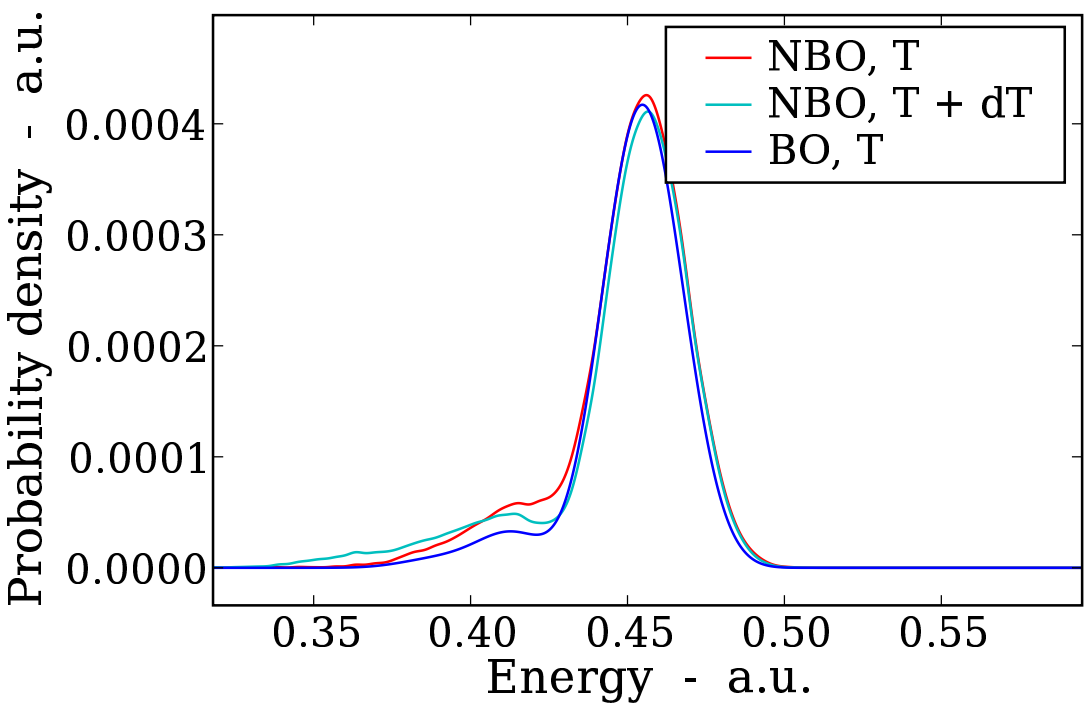

Figure 8.11: The KER spectra for protons after the ionisation of H_2^+ by a laser pulse with frequency $\omega = 0.355$ a.u. The non-BO spectrum will change with time in this basis, as demonstrated by the difference in shape between the spectrum where the time propagation is stopped immediately after the pulse, (red), and where the spectrum is propagated a few femtoseconds further, (cyan).

This problem occurs because we chose to do the analysis of the wavefunction in the BO basis. These are not the real eigenfunctions of the system, and the couplings between them do not disappear when $R \to \infty$. This can be shown, e.g. for the coupling between the electronic states ψ_e^1 and ψ_e^3, corresponding to potential curves $1g$ and $3g$. In the limit $R \to \infty$, the molecular electronic states, $\psi_e^i(x;R)$ will be linear combinations of hydrogen atomic states, $\psi_e^{Hi}(x \pm \frac{R}{2})$. The three lowest states will be

$$\psi_e^1(x;R) = \frac{1}{\sqrt{2}}\left[\psi_e^{H1}\left(x+\frac{R}{2}\right) + \psi_e^{H1}\left(x-\frac{R}{2}\right)\right]$$
$$\psi_e^2(x;R) = \frac{1}{\sqrt{2}}\left[\psi_e^{H1}\left(x+\frac{R}{2}\right) - \psi_e^{H1}\left(x-\frac{R}{2}\right)\right]$$
$$\psi_e^3(x;R) = \frac{1}{\sqrt{2}}\left[\psi_e^{H2}\left(x+\frac{R}{2}\right) + \psi_e^{H2}\left(x-\frac{R}{2}\right)\right]$$

The main non-BO coupling between ψ_e^3 and ψ_e^1 is

$$\left\langle \psi_e^3 \left| \frac{\partial}{\partial R} \right| \psi_e^1 \right\rangle_x =$$
$$\frac{1}{\sqrt{2}} \left\langle \psi_e^3 \left| \frac{\partial}{\partial R} \right| \left[\psi_e^{H1}\left(x + \frac{R}{2}\right) + \psi_e^{H1}\left(x - \frac{R}{2}\right) \right] \right\rangle_x \tag{8.1}$$

Using the chain rule, the differensiation may be rewritten as

$$\frac{\partial}{\partial R} f\left(x \pm \frac{R}{2}\right) = \pm \frac{1}{2} \frac{\partial}{\partial x} f\left(x \pm \frac{R}{2}\right)$$

when this is applied on Eq. (8.1) the problem may be reformulated as

$$\frac{1}{2}\frac{1}{\sqrt{2}} \left\langle \psi_e^3 \left| \frac{\partial}{\partial x} \right| \left[\psi_e^{H1}\left(x + \frac{R}{2}\right) - \psi_e^{H1}\left(x - \frac{R}{2}\right) \right] \right\rangle_x =$$
$$\frac{1}{2} \left\langle \psi_e^3 \left| \frac{\partial}{\partial x} \right| \psi_e^2 \right\rangle_x \neq 0$$

From parity considerations we know that this is an integral of an even integrand, and it will in general not be zero.

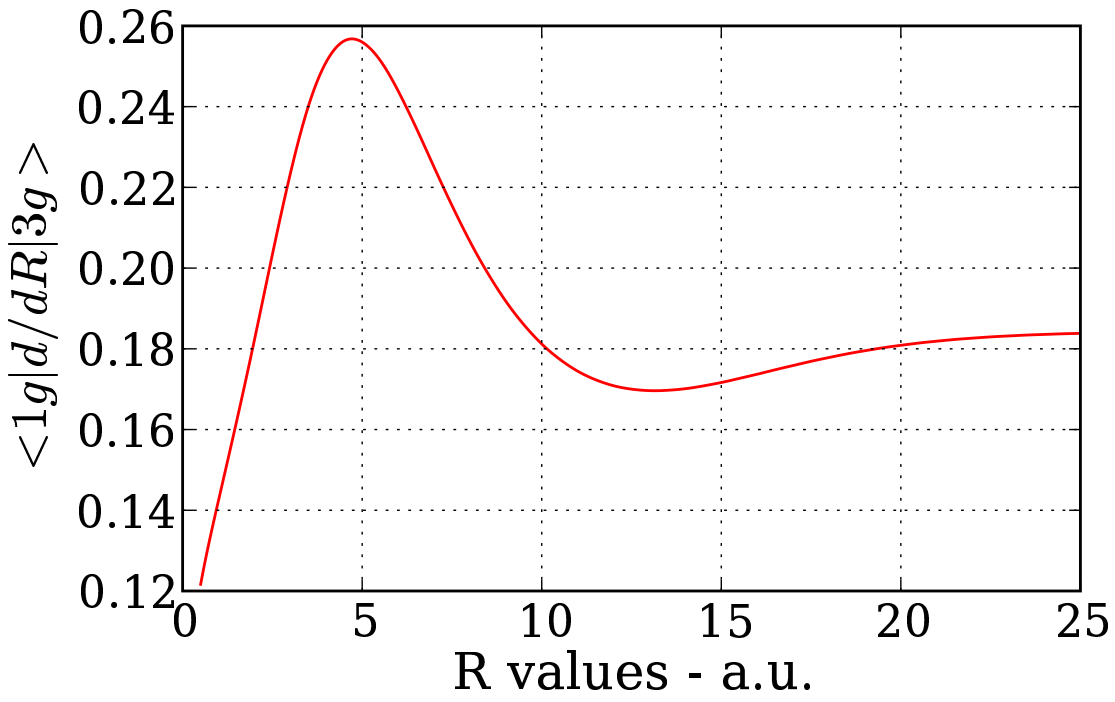

Figure 8.12: The non-BO coupling between the $1g$ and the $3g$ potential curves, $\left\langle \psi_e^1 \left| \frac{\partial}{\partial R} \right| \psi_e^3 \right\rangle_x$. The coupling does not go toward zero for large R values.

The same non-BO coupling calculated in our box, cf. Figure 8.12, shows no sign of disappearing for large R values. One would want all couplings to vanish asymptotically, as the atoms cannot perturb each other when infinitely far apart. We found the problem mentioned in an article concerning collisions [43, pp 307-321]. The problem is that when $\frac{\partial}{\partial R}\psi_e(x;R)$ is calculated, x is held fixed with respect to the centre of mass reference frame, rather than the reference frame of one of the nuclei. This leads to couplings of infinite range. In order to do proper analysis of the non-BO effects, one needs non-BO eigenstates with the correct asymptotic behaviour in the limit $R \to \infty$. Unforunately, solving the problem is not trivial [43, pp 312-321]. Resolving this issue could not be done in the thesis due to time concerns, but it is a natural choice for future work. To sum up, we have seen evidence that the BO approximation might break down, but in order to analyse our results, further work is needed.

Chapter 9

Conclusion and outlook

In the course of this thesis we have developed and tested a one dimensional model of the hydrogen molecular ion, H_2^+. In the first chapters we introduce the problem and some necessary theory about quantum mechanics, lasers, molecules and the Born-Oppenheimer approximation. In Chapter 4 we describe how to go from three dimensions to one dimension, and recount how additional steps were taken to improve the 1D model. In the next chapters we outline the numerical methods and the actual implementation of the model, before we in Chapter 7 and 8 describe how the model was tested against 3D simulations. The REMPI scenarios modelled in Chapter 7 reproduced the energy spectra of the 3D simulations well qualitatively, and the size of the results were of the same order. The finely tuned WPI scenarios studied in Chapter 8 were reproduced, albeit for slightly different laser settings, making it hard to compare the quantitative agreement. In general the model gives good qualitative results of comparable size to the 3D results. We ran into trouble with the non-Born-Oppenheimer calculations, and the calculations concerning such effects in this thesis should be considered as preliminary. To resolve the trouble, a proper descriptions of the physical non-BO states were needed. This turned out to be too extensive for the thesis, but solving the problem will be a natural continuation of this work. Another natural next step is the parallelisation of our program. With relative ease our code can be adapted to run on multiple processors. Setting up the Hamiltonian matrix consists of doing a lot of independent operations, and the execution of the program may be spread over many processors, thereby reducing the calculation time, and allowing us to build a larger basis. Fitting the electronic energy curves to the curves from the 3D model was a success. It would be interesting to try to extend this method to more electronic energy curves. In order to tackle even larger problems, we may consider doing the entire system propagation in the B-spline basis, rather than the eigenfunction basis. This would

complicate the analysis afterwards, but it would also allow us to look at a wide range of interesting problems.

Bibliography

[1] P. C. Hemmer. *Kvantemekanikk.* Tapir Akademisk Forlag, 2000. 1, 2.1, 3, 5.4, 6.2.2, 6.3

[2] H. F. Schaefer. *The electronic structure of atoms and molecules.* Addison-Wesley Publishing Co., 1972. 1

[3] B.H. Bransden and C.J. Joachain. *Physics of Atoms and Molecules.* Prentice Hall, 2003. 1, 1, 2.3, 2, 1

[4] A. H. Zewail. Femtochemistry: Atomic-scale dynamics of the chemical bond using ultrafast lasers (nobel lecture)13. *Angewandte Chemie International Edition*, 39:2586–2631, 2000. 1, 2.3

[5] Y. Silberberg. Ultrafast physics: Quantum control with a twist. *Nature*, 430:624, 2004. 1

[6] H. Rabitz, R. de Vivie-Riedle, M. Motzkus, and K. Kompa. Whither the future of controlling quantum phenomena? *Science*, 288(5467):824–828, 2000. 1, 2.3

[7] F. Martin, J. Fernandez, T. Havermeier, L. Foucar, Th. Weber, K. Kreidi, M. Schoffler, L. Schmidt, T. Jahnke, O. Jagutzki, A. Czasch, E. P. Benis, T. Osipov, A. L. Landers, A. Belkacem, M. H. Prior, H. Schmidt-Bocking, C. L. Cocke, and R. Dorner. Single Photon-Induced Symmetry Breaking of H_2 Dissociation. *Science*, 315(5812):629–633, 2007. 1

[8] Y. Hikosaka, T. Kaneyasu, E. Shigemasa, Y. Tamenori, and N. Kosugi. Autoionization dynamics of core-valence doubly excited states in N_2. *Physical Review A (Atomic, Molecular, and Optical Physics)*, 75(4):042708, 2007. 1

[9] S. Chelkowski, A. D. Bandrauk, A. Staudte, and P. B. Corkum. Dynamic nuclear interference structures in the coulomb explosion spectra of a hydrogen molecule in

intense laser fields: Reexamination of molecular enhanced ionization. *Physical Review A (Atomic, Molecular, and Optical Physics)*, 76(1), 2007. 1, 3.2, 4, 4.3

[10] M. Lein. Influence of molecular vibration on enhancements in high-order above-threshold ionization of hydrogen molecules. *Journal of Modern Optics*, 55(16):2631–2641, 2008. 1, 4

[11] C. C. Chirilă and M. Lein. High-order above-threshold ionization in stretched molecules. *Physical Review A (Atomic, Molecular, and Optical Physics)*, 74(5):051401, 2006. 1, 4

[12] M. Lein. Mechanisms of ultrahigh-order harmonic generation. *Phys. Rev. A*, 72(5):053816, Nov 2005. 1, 4

[13] A. Staudte, D. Pavičić, S. Chelkowski, D. Zeidler, M. Meckel, H. Niikura, M. Schöffler, S. Schössler, B. Ulrich, P. P. Rajeev, Th. Weber, T. Jahnke, D. M. Villeneuve, A. D. Bandrauk, C. L. Cocke, P. B. Corkum, and R. Dörner. Attosecond strobing of two-surface population dynamics in dissociating H_2^+. *Physical Review Letters*, 98(7):073003, 2007. 1, 4

[14] A. D. Bandrauk, S. Chelkowski, and I. Kawata. Molecular above-threshold-ionization spectra: The effect of moving nuclei. *Phys. Rev. A*, 67(1):013407, Jan 2003. 1, 4

[15] A. Palacios, S. Barmaki, H. Bachau, and F. Martín. Two-photon ionization of H_2^+ by short laser pulses. *Phys. Rev. A*, 71(6):063405, Jun 2005. 1, 4, 4, 7, 7.1, 7.2, 7.2, 1, 7.3

[16] M. Forre, S. Barmaki, and H. Bachau. Nuclear interference in the coulomb explosion of H_2^+ in short vuv laser fields. *Physical Review Letters*, 102(12), 2009. 1, 2.3, 4, 8, 8.2, 8.3, 8.7, 14, 14

[17] A. Einstein. Zur quantentheorie der strahlung. *Physikalische Gesellschaft Zurich*, 18:463–474, 1916. 2.3

[18] L. Garwin and T. Lincoln, editors. *A Century of Nature: Twenty-One Discoveries that Changed Science and the World*. University of Chicago Press, 2003. 2.3

[19] Nobelprize.org. http://nobelprize.org/nobel_prizes/physics/laureates/1997/index.html, 2009. 2.3

[20] E. Lillestøl, O. Hunderi, and J. R. Lien. *Generell Fysikk for Universitet og Høgskoler, bind 2*. Universitetsforlaget, 2001. 2

[21] M. Forre and H. Bachau. Orientation effects in the coulomb-explosion ionization of an H_2^+ wave packet by short xuv pulses: Applicability of the fixed-nuclei approximation. *Physical Review A (Atomic, Molecular, and Optical Physics)*, 77(5), 2008. 2.3

[22] S. Barmaki and H. Bachau. Coulomb explosion of H_2^+ wave packet in ultrashort XUV laser fields. *Journal of Physics B: Atomic, Molecular and Optical Physics*, 40(3):463–474, 2007. 2.3, 3

[23] M. Born and R. Oppenheimer. Zur quantentheorie der moleküle. *Annalen der Physik*, 84:457–484, 1927. 3

[24] K. Sändig, H. Figger, and T. W. Hänsch. Dissociation dynamics of H_2^+ in intense laser fields: Investigation of photofragments from single vibrational levels. *Phys. Rev. Lett.*, 85(23):4876–4879, Dec 2000. 3.2

[25] B. Feuerstein and U. Thumm. Fragmentation of H_2^+ in strong 800-nm laser pulses: Initial-vibrational-state dependence. *Phys. Rev. A*, 67(4):043405, Apr 2003. 3.2

[26] M. Vafaee. Nuclear kinetic energy spectra of D_2^+ in an intense laser field: Beyond the born-oppenheimer approximation. *Physical Review A (Atomic, Molecular, and Optical Physics)*, 78(2):023410, 2008. 4

[27] V. Roudnev, B. D. Esry, and I. Ben-Itzhak. Controlling HD^+ and H_2^+ dissociation with the carrier-envelope phase difference of an intense ultrashort laser pulse. *Phys. Rev. Lett.*, 93(16):163601, Oct 2004. 4, 4.3

[28] Feng He, C. Ruiz, and A. Becker. Control of electron excitation and localization in the dissociation of H_2^+ and its isotopes using two sequential ultrashort laser pulses. *Physical Review Letters*, 99(8):083002, 2007. 4

[29] S. Chelkowski, A. Conjusteau, T. Zuo, and A. Bandrauk. Dissociative ionization of H_2^+ in an intense laser field: Charge-resonance-enhanced ionization, coulomb explosion, and harmonic generation at 600 nm. *Phys. Rev. A*, 54(4):3235–3244, Oct 1996. 4

[30] S. Barmaki and H. Bachau. Coulomb explosion of H_2^+ wave packet in ultrashort xuv laser fields. *Journal of Physics B: Atomic, Molecular and Optical Physics*, 40(3):463–474, 2007. 4

[31] S. Selstø, A. Palacios, J. Fernández, and F. Martín. Electron angular distribution in resonance-enhanced two-photon ionization of H_2^+ by ultrashort laser pulses. *Physical Review A (Atomic, Molecular, and Optical Physics)*, 75(3):033419, 2007. 4, 7

[32] A. Palacios, H. Bachau, and F. Martin. Resonant effects in the coulomb explosion of H_2^+ by ultrashort laser pulses. *Journal of Physics B: Atomic, Molecular and Optical Physics*, 38(6):L99–L105, 2005. 4, 7

[33] Python programming language – official website. http://www.python.org/, 2009. 4.2

[34] J. M. Peek. Eigenparameters for the $1s\sigma_g$ and $2p\sigma_u$ Orbitals of H_2^+. *J. Chem. Phys.*, 43:3004–3007, 1965. 4.2, 4.1

[35] W. Cheney. *Analysis for Applied Mathematics*. Springer, 2001. 1, 6.2

[36] S. A. Sørngård. Lifetimes of excited states of quantum dot molecules. Master's thesis, University of Bergen, Norway, 2009. 5.2

[37] C. de Boor. *A Practical Guide to Splines*. Springer-Verlag, New York, 2001. 5.3

[38] H. Bachau et al. Applications of B-splines in atomic and molecular physics. *Rep. Prog. Phys.*, 64:1815–1943, 2001. 8, 5.2

[39] C. F. Gerald and P. O. Wheatly. *Applied Numerical Analysis*. Addison-Wesley Publishing Company, New York, 7 edition, 2004. 9, 5

[40] D. Kincaid and W. Cheney. *Numerical Analysis: Mathematics of Scientific Computing*. Brooks/Cole, 2002. 5.4

[41] All project source code, at SVN repository. http://svn.uib.no/cqp/public/software/python-bsplines/trunk/H2Plus/, 2009. 6.1

[42] L. F. Shampine and M. K. Gordon. *Computer Solution of Ordinary Differential Equations: the Initial Value Problem*. W. H. Freeman, San Francisco, 1975. 6.2

[43] John B. Delos. Theory of electronic transitions in slow atomic collisions. *Rev. Mod. Phys.*, 53(2):287–357, Apr 1981. 8.4